SUSTAINABLE FINANCE PROGRAMME

SSEE

UNIVERSITY OF OXFORD

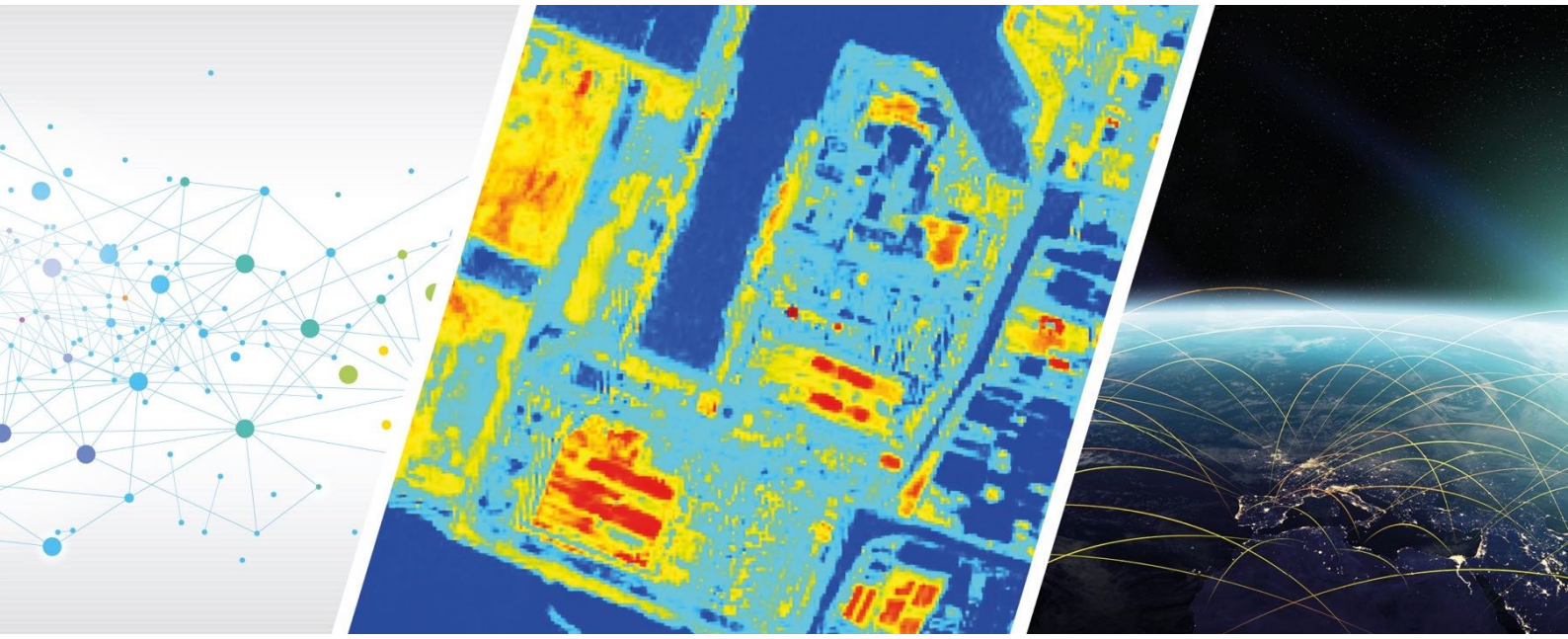

Climate risk analysis from space: remote sensing, machine learning, and the future of measuring climate-related risk

Report

July 2018

In Partnership with:

GFZ POTSDAM

CARBON DELTA

eit Climate-KIC

About

About the Consortium

Oxford Sustainable Finance Programme

The Oxford Sustainable Finance Programme at the University of Oxford Smith School of Enterprise and the Environment is a multidisciplinary research centre working to be the world's best place for research and teaching on sustainable finance and investment. The Programme was established in 2012 to understand the requirements, challenges, and opportunities associated with a reallocation of capital towards investments aligned with global environmental sustainability.

The Programme is based in a world leading university with a global reach and reputation. We work with leading practitioners from across the investment chain (including actuaries, asset owners, asset managers, accountants, banks, data providers, investment consultants, lawyers, ratings agencies, stock exchanges), with firms and their management, and with experts from a wide range of related subject areas (including finance, economics, management, geography, anthropology, climate science, law, area studies, psychology) within the University of Oxford and beyond.

Carbon Delta

Carbon Delta has performed a considerable amount of research on the availability of climate risk data and the expertise needed to maximise the outcomes of such a project. Carbon Delta is a climate research firm that specialises in identifying and analysing the climate change resilience of publicly traded companies. Furthermore, Carbon Delta has developed a database of company locations for 25,000 enterprises.

Carbon Delta provides coordinates for millions of production installations, processes satellite imagery and integrates data and runs assessment methodologies. When processing the satellite imagery, Carbon Delta will develop a 3-dimensional understanding of the technological activity happening at facilities for potentially thousands of companies.

German Research Centre for Geosciences (GFZ)

The Helmholtz-Zentrum Potsdam - German Research Centre for Geosciences (GFZ) is the German National Research Centre for Earth sciences and a member of the German Helmholtz Association (HGF). One of the GFZ methodical core competences are in application and development of satellite technologies and spacebased measuring methods to monitor Earth surface variables and processes from a range of spatial and temporal scales using in-situ, airborne and space-borne instruments. The GFZ Remote Sensing section focuses on the development and use of remote sensing techniques for the monitoring of land surfaces. In particular, research lines comprise (i) methodological developments for remote sensing data analysis and definition of future satellite missions, and (ii) application-oriented research for the monitoring of bio- and geophysical parameters of interest to a wide range of scientific disciplines, including land degradation studies, natural resources, global vegetation functioning, and land-atmosphere interactions. In particular, the remote sensing section is renowned for its expertise in hyperspectral remote sensing and is the scientific leader of the EnMAP hyperspectral satellite sensor to be launched in 2019.

Project funded via EIT Climate-KIC's CSA Booster

This innovative project has been made possible through seed-funding from EIT Climate-KIC via CSA Booster (http://csabooster.climate-kic.org), a flagship programme of its Sustainable Land Use theme. EIT Climate-KIC is a European knowledge and innovation community, working to accelerate the transition to a zero-carbon economy. Supported by the European Institute of Innovation and Technology, it identifies and supports innovation that helps society mitigate and adapt to climate change.

Climate-KIC's CSA Booster is Europe's leading innovation hub, community and collaboration platform pioneering the transition to climate-smart agriculture across Europe, and around the world. Established in 2015, CSA Booster brings together a multi-stakeholder ecosystem of public and private sector partners including some of the leading research institutions in Europe, corporates, start-ups and international organizations to catalyse, incubate and scale innovative CSA solutions and to de-risk investments into CSA. CSA Booster has partners and projects in all major EU regions and currently acts as the European regional hub for the Global Alliance for Climate-smart Agriculture (GACSA) initiative, hosted by the UN's Food and Agriculture Organisation (FAO).

About the Authors

Oxford Sustainable Finance Programme

Dr Ben Caldecott is the founding Director of the Oxford Sustainable Finance Programme at the University of Oxford Smith School of Enterprise and the Environment. He is concurrently an Academic Visitor at the Bank of England, a Visiting Scholar at Stanford University, a Senior Advisor at Highmore LLC, and a Senior Associate Fellow at Bright Blue. Ben specialises in environment, energy, and sustainability issues and works at the intersection between finance, government, civil society, and academe, having held senior roles in each domain.

Lucas Kruitwagen is the Data Lead at the Oxford Sustainable Finance Programme and a D.Phil. Student in the University of Oxford School of Geography and the Environment. Lucas researches how data-driven technology is changing the availability of environmental risk information, particularly in relation to company and investor risk exposure. Lucas is also a Visiting Researcher at Imperial College London where he researches organisational decision-making under conditions of risk and uncertainty. He holds an MSc (with distinction) in Sustainable Energy Futures from Imperial College London where he was a ClimateKIC Master's Label Student, and a BEng from McGill University, Montreal, where he was a Loran Scholar.

Dr Matthew McCarten is a Postdoctoral Research Associate at the Oxford Sustainable Finance Programme. Prior to joining Oxford he completed his PhD thesis in finance at the University of Otago, New Zealand in 2017. His thesis examined the determinants and consequences of securities class actions. In particular, investigating the association between securities class actions and various corporate characteristics, including debt financing, political lobbying and innovation. He also holds a MBus (with distinction) and a BCom from the University of Otago.

Dr Xiaoyan Zhou is a Postdoctoral Research Associate at the Oxford Sustainable Finance Programme. Her research interests focus on Responsible Investment, Carbon Disclosure/Emission and Institutional Shareholder Engagement. Prior to joining the Sustainable Finance Progamme, Xiaoyan Zhou was in charge of establishing two joint venture companies in China and fully participated two IPOs on Australian Stock Exchange and London Stock Exchange Alternative Investment Market during 2003-2007. She holds a PhD in Finance from ICMA Centre, Henley Business School and MLitt in Finance and Management from University of St Andrews.

Carbon Delta

David Lunsford is a Co-Founder and Head of Development for Carbon Delta, where he designs risk assessment methodologies, manages a team of research analysts, oversees and validates analytical results, and builds client relationships for the firm. He previously worked for several years on climate change mitigation and greenhouse gas trading issues in Europe and China, supporting large companies in managing climate risks associated with the transition to a low carbon economy. David possesses 11 years of experience bringing diverse stakeholders together on varying levels, encouraging new climate change strategies that make sense for business, investors and policymakers alike.

Oliver Marchand is a Co-Founder and CEO of Carbon Delta. Prior to this, he spent 9 years with Fisch Asset Management as Head of IT. In that position he led a team that was responsible for all IT operations and development of the in-house portfolio management system. Moreover, Oliver worked as a researcher in weather forecasting for almost a decade at various weather services. This included exciting research projects such as the development of thunderstorm warning systems and wind profiling data integration, and required a high-performance computing cluster operation. Oliver holds a Ph.D. in Computer Science from ETH Zürich. He is passionate about programming, triathlon, solar cooking and his family.

Phanos Hadjikyriakou is a Data Analyst at Carbon Delta. He is working on methods to approximate supply chain information, using multi-regional input-output analysis. Part of his research includes water accounting, natural capital valuation and scope 3 carbon footprints. Phanos is passionate about using

macro-economic data to increase the transparency of global supply chains and quantify their environmental impacts. He studied at the ETH Lausanne and Zurich and will soon graduate with a Masters in Environmental Engineering.

Valentin Bickel is a PhD student at the Swiss Federal Institute of Technology Zurich (Switzerland) and the Max Planck Institute for Solar System Research in Göttingen (Germany), working in the field of Remote Sensing and Planetary Science. He joined the Carbon Delta team as an external consultant.

German Research Centre for Geosciences (GFZ)

Prof. Dr. Torsten Sachs is the head of the Earth-Atmosphere Interactions Group within the GFZ Section Remote Sensing. His research focusses on the land-atmosphere exchange of heat, water vapor, and greenhouse gases (CO2, CH4) from local (m² - ha) to regional (>10.000 km²) scales using stationary and mobile (airborne) platforms in both temperate and high latitudes. He has 14 years of research experience including eight extensive aircraft and helicopter-based campaigns in the US, Canadian, and Siberian Arctic as well as northern Scandinavia. Among other projects, he is involved in the EU Horizon2020 Research and Innovation Actions INTAROS and NUNATARYUK, as well as in the Cofund ERA-NETs ERA-GAS and ERA-PLANET. He serves in the Science Advisory Group of the German-French Methane Remote Sensing LIDAR (MERLIN) Mission to be launched in June 2020.

Niklas Bohn is a PhD candidate at GFZ Postdam undertaking work in the remote sensing section. Niklas has also worked as a research assistant and interned at GFZ between 2016 and 2017. He has also interned at the United Nations Platform for Space-based Information for Disaster Management and Emergency Response (UN-SPIDER). He holds a Master of Science in Studies of Environmental Geography and Management.

Disclaimer

Contents

Executive Summary

- Accurate asset-level data can dramatically enhance the ability of investors, regulators, governments, and civil society to measure and manage different forms of environmental risk, opportunity, and impact. Asset-level data is information about physical and non-physical assets tied to company ownership information.
- Remote sensing (and related technological developments such as machine learning) can help secure better asset-level data and at higher refresh rates. In particular remote sensing can help identify the features and use of assets relevant to determining asset-level GHG emissions.
- **We expect that the development of a global catalogue of every physical asset in the world to be already within the reach of technical feasibility.** The process of identifying and tagging assets (e.g. power generating stations, mines, farms, industrial sites) and asset-level features (e.g. cooling technologies, air pollution control technologies) can be automated through the use of machine learning.
- **It is possible to train learning algorithms to recognise an asset and its features in remote imagery and then scan global imagery corpuses to identify all assets of that type.** Human error rates are sufficiently low on these classification tasks that it is reasonable to expect these problems to be entirely automatable.
- **With the exponential increase in space-based sensing, computing power, and algorithmic complexity, end-to-end learning systems are becoming increasingly available** to academic researchers and the private sector alike.
- **There are also viable methods using remote sensing data that could be implemented to measure asset-level GHG emissions**. These methods are: (1) a direct method, which involves the use of various sensors on spaceborne and airborne instruments to measure emissions directly; and (2) an indirect method, which utilises various identifiable asset characteristics to model GHG emissions.
- The direct method of monitoring emissions requires the use of satellite or airborne instruments. Accurately monitor GHGs from space is challenging because of their relatively small signal in comparison to other atmospheric constituents, but advances in both sensor technology and retrieval models are leading to more precise detection.
- Direct emission monitoring is currently feasible for a relatively limited scope of assets (such as assets that are situated in regions with very few other sources of emissions in the surrounding area). **The launch of the CarbonSat satellite in 2020 as well as some already scheduled sun-synchronous sensors offer the potential for more precise observation of GHG concentrations and emissions at the asset-level.**
- **A complementary approach to direct measurement is to model GHG emissions indirectly using identifiable asset characteristics.** This requires the identification of key characteristics that are associated with GHG emissions. For example, asset utilisation rates are inherently linked to the level of GHG emissions. Using some of the spaceborne instruments in combination with real asset-level production data it is possible to model an asset's utilisation rate. Employing this projection of the utilisation rate an estimate of the emissions can then be obtained using a standardised model. **The indirect approach represents a more feasible method of measuring GHG emissions based on currently available technology.**
- **Through future research projects undertaken over multiple phases we plan to make asset-level data (including various technical features) and GHG emissions monitoring for each asset (using both direct and indirect methods) available for every physical asset in every sector globally, beginning with the most GHG intensive assets.** We hope to create platforms for various users to access and use this data. This endeavour has the potential to transform how different actors in different parts of society measure and manage environmental risks, impacts and opportunities. It is enabled by significant public (and private) investment in data capture and remote sensing, which can now be brought together and processed in novel ways for direct application.

1. Introduction

Accurate asset-level data can dramatically enhance the ability of investors, regulators, governments, and civil society to measure and manage different forms of environmental risk, opportunity, and impact. Asset-level data is information about physical and non-physical assets tied to company ownership information. Asset-level data can be aggregated at the company, regional, or global level suiting a variety of needs, for example:

- **Asset managers** want data that can be analysed so as to differentiate between companies. They would like to be able to do that across asset classes (e.g. equities, non-listed, corporate bonds etc.), sectors (e.g. downstream energy, upstream energy, transport, property etc.), and markets (e.g. US, China, EU etc.). Companies own portfolios of assets and so understanding the exposure of company assets to environmental factors and aggregating this data to the parent company-level is the best way of understanding firm wide exposure.
- In turn, **asset owners** want to be able to know the exposure of their asset managers so they can differentiate between them and compare them to benchmarks. If we know who owns which companies, and we know how exposed each company asset is to different risks, then we can effectively analyse asset manager exposure.
- **Citizen savers** are increasingly concerned about ethical considerations and trends such as the fossil fuel divestment campaign. They want to know which asset owners and which fund options are most aligned with their concerns and priorities. This trend is accelerating due to the trend towards 'Defined Contribution' pension schemes opposed to more traditional 'Defined Benefit' ones.
- **Regulators**, as recently demonstrated by interventions from the Governor of the Bank of England and others, are interested in where risk is in the system and whether it could have financial stability implications if there is a disorderly correction due to rapid changes in asset prices. They want to see which entities own assets most at risk – for example, which systemically important financial institutions are exposed directly or indirectly to particularly at risk assets.
- Finally, **policymakers and civil society** want to know whether we are on track to delivering the transition to a low carbon economy, whether in aggregate (e.g. globally, regionally, nationally) or in terms of specific companies or sectors within countries. To do this, they need to know how much 'committed emissions' there are from existing assets or will be from planned capital expenditure. Civil society will want to examine whether companies' rhetoric and action add up, and also whether financial institutions own or are financing companies and assets that are incompatible with climate change and other environmental challenges.

Asset-level data resides in a wide range of different locations. It exists in current company disclosures to financial markets, regulators, and government agencies (in multiple jurisdictions and in different languages); in voluntary disclosures; in current proprietary and non-proprietary databases; in public and private research institutions; and in academic research. Despite this, it is often of very poor quality, in terms of both coverage and accuracy. As a result, the use of remote sensing to identify asset-level data can significantly improve our understanding of asset-level risks.

This report examines the potential role of remote sensing (and related technological developments such as machine learning) to secure better asset-level data and at higher refresh rates. In particular we focus on using remote sensing to identify the features and use of assets relevant to determining their greenhouse gas (GHG) emissions. Remote sensing combined with machine learning could potentially provide the ability to:

- Conduct 'persistent' monitoring of assets;
- Significantly enhance the determination of asset ownership;
- Facilitate satellite measurement of asset-level greenhouse gas (GHG) emissions;
- Allow the 'real time' monitoring and identification of local environmental impacts;

- Make data and analysis available to a wide range of stakeholders helping to ensure that the more sophisticated approaches benefit to society as a whole; and
- Combine remote sensing environmental risk analysis with large scale financial databases to develop innovative products.

1.1. Questions

As part of our research we focused on the following questions:

- What is the accessibility of high resolution satellite data offered via non-commercial satellites to measure GHG emissions from large emitting assets?
- What data products are offered by other, possibly commercial, data providers to measure GHG?
- What is the accessibility of high resolution remote sensing data to identify technology features of assets?
- What is the feasibility of developing a methodology for asset-level GHG measurement through remote sensing?
- What is the feasibility of developing a methodology for identifying technology features of assets?

The report is organised as follows. Section 2 provides an overview of the data sources that are available and the methods that can be implemented for the identification of asset-level technology features. Section 3 outlines two potential methods for measuring GHG emissions. These methods are: (1) a direct method, which involves the use of various sensors on spaceborne and airborne instruments to measure emissions directly; and (2) an indirect method, which utilises various identifiable asset characteristics to model GHG emissions. Section 4 outlines a method to automatically identify an assets environment and presents an approach for using OpenStreetMaps to identify the location of assets. In Section 5 a pilot study analysing the feasibility of identifying types of assets and their features from space is reported. Finally, Section 6 provides concluding remarks.

2. Identifying Technology Features at Assets

Many human-made assets have features that indicate their actual or potential impact on the natural environment, as well as the exposure of an asset to different environment-related risks (and opportunities).

For example, assets in locations with high population density, serious local air pollution, and which lack emissions abatement are at greater risk of being regulated and required to either install emission abatement technologies or cease operation. Assets that utilise emission abatement technologies (e.g. flue gas desulphurisation units and electrostatic precipitators) will have lower emissions and also face lower financial risks.

Furthermore, assets located in areas with higher physical baseline water stress are at higher risk of being forced to reduce or cease operations. This water stress risk will be lower for assets deploying water-efficient cooling systems, such as utilising closed-cycle, hybrid or dry-cooling technology.

Finally, the more carbon intensive an asset is the more likely it is to be negatively impacted by climate policy, in terms of carbon pricing, emissions performance standards, or other similar measures. More carbon-intensive assets are more exposed to transitional risk from climate change mitigation policy. More efficient production technology (such as the type of boiler used in power plants) can significantly reduce the carbon intensity of an asset and as a result also reduce its risk exposure.

Methods for identifying these features can give researchers and others access to large-scale datasets of assets in the real economy and their features relevant to objectively measuring environmental risks and impacts.

2.1. Data Availability

Currently, we can identify features by examining satellite imagery provided by sources such as Google Earth and manually tagging asset specific locations and classifying them into various groups. This type of identification process has been used by CoalSwarm who have developed a database of coal-fired power plants. To determine exact coordinates for power plants CoalSwarm used Google Maps, Google Earth, or Wikimapia. This type of manual classification and tagging becomes particularly onerous if there is no easy way to identify, generally, where assets are located.

This process of identifying and tagging assets can be done in a more efficient manner through the using of machine learning. Machine learning applies statistical techniques to a corpus of data to 'learn' the parameters of a sophisticated classification or regression algorithm. Computer vision describes a class of problem where machine learning has been successfully applied to recognising object and features in images. These methods might be applied to a global corpus remote sensing imagery, enabling the detection and feature extraction of assets anywhere in the world. Using this type of process it is possible to build a global catalogue of physical assets.

One of the challenges facing remotely-sensed environmental feature detection is the lack of labelled training data. It is yet indeterminate whether a generalizable feature detection machine can be built from a relatively small seeded sample of real economy assets and their environmental features. Major breakthroughs in computer vision occurred when the number of images in the training set was expanded from thousands to millions and the neural network architecture used in their analysis extended to dozens of layers. There are promising methods for overcoming these data problems.

Conventional data science techniques such as data synthesis and resampling can artificially reduce model error in exchange for bias. While a form of data synthesis, time-series remote sensing imagery can improve data availability beyond crude data synthesis and resampling. Transfer learning has been successfully applied to build reliable classifiers with training samples on the order of 1000s. There is no shortage of remote sensing data – rather a shortage of labels. Most neural-network classifiers of remote sensing imagery do not use all multi-spectral bands of data. Open-source geospatial data such as OpenStreetMaps might be used to train networks capable of ingesting all spectra of imagery, which can

then be transferred for more specific classification tasks. As a final resort, the previous literature of hand-crafted features can be consulted.

2.2. Algorithms

Asset detection in remote sensing imagery began as a collection of conventional methods in Geographic Information Systems (GIS).[1] Assets are identified by an algorithmic collection of features (such as edges, gradients, shapes, and colours), which in turn are patterns in the underlying image data. In the past, the formulae for the identification of features were done by a researcher by hand, perhaps with the assistance of a statistical model.[2] With coarse resolutions, assets were often sub-pixel in scale; features involved band math of single pixels or the close neighbourhood of pixels.[3]

Machine learning methods have been used for several decades to support the development of features in asset detection. In the absence of sufficient data, computing power, and algorithm research, researchers used low-complexity methods like random-forests[4] or support vector machines[5] to build passable classifiers, sometimes utilising hand-designed band-math features as inputs or logic heuristics as outputs.[6] As a general rule, where researchers have encountered data, algorithmic, or computing barriers they have hand-developed the feature math or heuristic logic themselves. Emerging machine learning methods are rendering this design work obsolete.

Deep learning computer vision methods are now making their entry into the remote sensing field.[7] Remote sensing computer vision problems are somewhat unique as a class – in some ways which are advantageous such as fixed perspectives (i.e. zenith angles and orbit distances) and the availability of multi-spectral data, and others which present unique challenges (e.g. cloud interference). Convolutional neural networks (CNNs) are the leading method for image classification, taking into account the 2-dimensional 'proximity' of pixels in their input features.[8] CNNs can learn sophisticated features of the input image, including pixel-by-pixel semantic segmentation, identifying objects and object features in the image.[9] Generalised multi-class classifiers can be used across asset types to improve training efficiency.

Environmental features of technology may be learnable like any other features of an asset class of interest. Indeed, that a human expert can recognise, in a suitably high-resolution image, certain environmental features indicates that the Bayesian error for such a task is not so high as to prevent the useful automation of feature detection. As computing power, data availability, and algorithm sophistication grow exponentially, more and more sophisticated feature detection problems become possible. One of the purposes of this present study is to benchmark progress on solving these problems, and be able to project when progress will unlock the ability to solve problems relevant to the analysis of climate-related risk.

[1] See, e.g., Blashke, T. (2010),' Object based image analysis for remote sensing', *ISPRS Journal of Photogrammetry and Remote* Sensing 65(1), 2-16.
[2] Tokarczyk, P., Wegner, J. D., Walk, S., & Schindler, K. (2013) 'ISPRS Annals of Photogrammetry, Remote Sensing and Spatial Information Sciences', II-3W1
[3] See, e.g., Kerekes, J. P. (2011) 'Hyperspectral remote sensing subpixel object detection performance', Applied Imagery Pattern Recognition Workshop (AIPR), Washington DC, 2011, pp. 1-4.
[4] See, e.g., Freidl, M. A., & Brodley, C. E. (1997) 'Decision tree classification of land cover from remotely sensed data', *Remote Sensing* of Environment, 399-409.
[5] See, e.g., Melgani, F., & Bruzzone, L. (1993) 'Classifciation of Hyperspectral Remote Sensing Images with Support Vector Machines', *IEEE Transactions Geoscience and Remote Sensing*, 42(8) 1778-1790.
[6] See Niemeyer, I. & Canty, M. J. (2001), Knowledge-based interpretation of satellite data by object-based and multi-scale image analysis in the context of nuclear verification, in 'Geoscience and Remote Sensing Symposium, 2001', pp. 2982–2982.
[7] Cheng, G. & Han, J. (2016), 'A survey on object detection in optical remote sensing images', *ISPRS Journal of Photogrammetry and Remote Sensing*, 117, 11–28.
[8] See, e.g., Romero, A., Gatta, & C., Camps-Valls, G. (2015) 'Unsupervised Deep Feature Extraction for Remote Sensing Image Classification', *IEEE Transactions on Geoscience and Remote Sensing*, 54(3), 1349 - 1362
[9] See, e.g., Yiting, T., Xu, M., Zhang, F., & Zhang, L. (2017) 'Unsupervised-Restricted Deconvolutional Neural Network for Very High Resolution Remote-Sensing Image Classification', *IEEE Transactions on Geoscience and Remote Sensing*, PP(99):1-19

Table 1. Identification of Human-Made Assets and Features
This table presents a summary of the various features that have been identified remotely within different sectors.

Sector	Identified Features
Buildings	Building Detection,[10] Building Height Estimation[11]
Road/Rail	Centerline/Network Extraction,[12] Environmental Exposure[13]
Aviation	Aircraft Detection[14]
Shipping	Ship Detection[15]
Automotive	Car Detection[16]
Heavy Industry	Bauxite Pollution Detection[17]
Mining	Underground Mining Detection,[18] Environmental Monitoring[19]
Oil & Gas	Oil Spill Detection,[20] Gas Flaring Detection and Volume Estimation,[21] Offshore Platform Detection[22]
Utilities	Wind Resource Assessment,[23] Wind Turbine Detection,[24] Solar PV Detection[25]

[10] Cote, M. & Saeedi, P. (2013), 'Automatic rooftop extraction in nadir aerial imagery of suburban regions using corners and variational level set evolution', *IEEE Transactions on Geoscience and Remote Sensing* 51(1), 313–328.
[11] Colin-Koeniguer, E. & Trouva, N. (2014), 'Performance of building height estimation using high-resolution polinsar images', *IEEE Transactions on Geoscience and Remote Sensing* 52(9), 5870–5879.
[12] Hu, X., Li, Y., Shan, J., Zhang, J. & Zhang, Y. (2014), 'Road centerline extraction in complex urban scenes from lidar data based on multiple features', *IEEE Transactions on Geoscience and Remote Sensing* 52(11), 7448–7456.
[13] Chen, F., Lin, H., Li, Z., Chen, Q. & Zhou, J. (2012), 'Interaction between permafrost and infrastructure along the qinghai-tibet railway detected via jointly analysis of c- and l-band small baseline {SAR} interferometry', *Remote Sensing of Environment* 123, 523–540.
[14] Zhang, F., Du, B., Zhang, L. & Xu, M. (2016), 'Weakly supervised learning based on coupled convolutional neural networks for aircraft detection', *IEEE Transactions on Geoscience and Remote Sensing* 54(9), 5553–5563.
[15] Zou, Z. & Shi, Z. (2016), 'Ship detection in spaceborne optical image with svd networks', *IEEE Transactions on Geoscience and Remote Sensing* 54(10), 5832–5845.
[16] Chen, Z., Wang, C., Wen, C., Teng, X., Chen, Y., Guan, H., Luo, H., Cao, L. & Li, J. (2016), 'Vehicle detection in high-resolution aerial images via sparse representation and superpixels', *IEEE Transactions on Geoscience and Remote Sensing* 54(1), 103–116.
[17] Pascucci, S., Belviso, C., Cavalli, R. M., Palombo, A., Pignatti, S. & Santini, F. (2012), 'Using imaging spectroscopy to map red mud dust waste: The podgorica aluminum complex case study', *Remote Sensing of Environment* 123, 139–154.
[18] Hu, Z., Ge, L., Li, X., Zhang, K. & Zhang, L. (2013), 'An undergroundmining detection system based on dinsar', *IEEE Transactions on Geoscience and Remote Sensing* 11(1), 615–625.
[19] Zhang, B., Wu, D., Zhang, L., Jiao, Q. & Li, Q. (2012), 'Application of hyperspectral remote sensing for environment monitoring in mining areas', *Environmental Earth Sciences* 65(3), 649–658.
[20] Maio, A. D., Orlando, D., Pallotta, L. & Clemente, C. (2017), 'A multifamily glrt for oil spill detection', *IEEE Transactions on Geoscience and Remote Sensing* 53(1), 63–79.
[21] Anejionu, O. C., Blackburn, G. A. & Whyatt, J. D. (2015), 'Detecting gas flares and estimating flaring volumes at individual flow stations using {MODIS} data', *Remote Sensing of Environment* 158, 81–94.
[22] Liu, Y., Sun, C., Yang, Y., Zhou, M., Zhan, W. & Cheng, W. (2016), 'Automatic extraction of offshore platforms using time-series landsat-8 operational land imager data', *Remote Sensing of Environment* 175, 73–91.
[23] Doubrawa, P., Barthelmie, R. J., Pryor, S. C., Hasager, C. B., Badger, M. & Karagali, I. (2015), 'Satellite winds as a tool for offshore wind resource assessment: The great lakes wind atlas', *Remote Sensing of Environment* 168, 349–359.
[24] Vanhellemont, Q. & Ruddick, K. (2014), 'Turbid wakes associated with offshore wind turbines observed with landsat 8', *Remote Sensing of Environment* 145, 105–115.
[25] Bradbury, K., Saboo, R., Johnson, T. L., Malof, J. M., Devarajan, A., Zhang, W., Collins, L. M. & Newell, R. G. (2016), 'Distributed solar photovoltaic array location and extent dataset for remote sensing object identification', *Scientific Data* 3(1), 1–9.

3. Measuring GHG Emissions

The monitoring of atmospheric greenhouse gas (GHG) concentrations from space is becoming increasingly important since they drive climate change. More than 40% of global annual anthropogenic CO_2 emissions are caused by coal burning power plants and CH_4 is emitted by both anthropogenic sources like livestock, oil-gas systems, landfills, coal mines, wastewater management and rice cultivation, as well as by natural sources like wetlands, inland waters and termites.[26, 27, 28, 29] CH_4 has a 100 year Global Warming Potential (GWP) approximately 21 times that of CO_2.[30]

This section provides an overview of two possible methods that could be implemented to measure GHGs. These methods are: (1) a direct method, which involves the use of various sensors on spaceborne and airborne instruments to measure emissions directly; and (2) an indirect method, which utilises various identifiable asset characteristics to model GHG emissions.

3.1. Direct Emissions Monitoring

The direct method of monitoring emissions requires the use of satellite or airborne instruments. Accurately monitoring GHGs from space is challenging because of their relatively small signal in comparison to other atmospheric constituents, but advances in both sensor technology and retrieval models are leading to more precise detection. Higher spatial resolution, in particular, is critical in order to quantify emissions from point sources like coal mines, ventilation shafts or landfills.[31] The following section presents an overview of the various spaceborne and airborne instruments available for GHG measurement; the retrieval methods that could be applied; the detection thresholds and precision of the retrievals; and finally provides concluding remarks on the feasibility of the direct method of emissions measurement.

3.1.1. Available Instruments

3.1.1.1. Spaceborne Instruments

Since the launch of SCIAMACHY in 2003 spaceborne instruments have been able to retrieve measures of atmospheric CO_2 and CH_4. Depending on the instrument, the retrievals can be obtained at a global scale or at the asset-level in combination with airborne data. Generally, satellite sensors are in a low sun-synchronous orbit, which leads to a fixed observing time each day for every point on the surface of the earth. CO_2 and CH_4 are detected as column-averaged dry air mole fractions (XCO_2, XCH_4) in the along-

[26] Nassar, R., Hill, T. G., McLinden, C. A., Wunch, D., Jones, D. B. A., & Crisp, D. (2017). 'Quantifying CO2 Emissions From Individual Power Plants From Space'. *Geophysical Research Letters*, 44(19), 10,045-10,053.
[27] Jacob, D. J., Turner, A. J., Maasakkers, J. D., Sheng, J., Sun, K., Liu, X., Chance, K., Aben, I., McKeever, J., & Frankenberg, C. (2016). 'Satellite observations of atmospheric methane and their value for quantifying methane emissions'. *Atmospheric Chemistry and Physics*, 16(22), 14371-14396.
[28] Ehret, G., Bousquet, P., Pierangelo, C., Alpers, M., Millet, B., Abshire, B. J., Bovensmann, H., Burrows, P. J., Chevallier, F., Ciais, P., Crevoisier, C., Fix, A., Flamant, P., Frankenberg, C., Gibert, F., Heim, B., Heimann, M., Houweling, S., Hubberten, W. H., Jöckel, P., Law, K., Löw, A., Marshall, J., Agusti-Panareda, A., Payan, S., Prigent, C., Rairoux, P., Sachs, T., Scholze, M., & Wirth, M. (2017). 'MERLIN: A French-German Space Lidar Mission Dedicated to Atmospheric Methane'. *Remote Sensing*, 9(10).
[29] Termites produce methane as a by-product of their digestive process, which is a result of the symbiotic and protozoaic bacteria present in their digestive system.
[30] Houghton, J. T., Meira Filho, L. G., Callander, B.A., Harris, N., Kattenberg, A. & Maskell, K. (1996). Climate change 1995: The science of climate change: contribution of working group I to the second assessment report of the Intergovernmental Panel on Climate Change. Vol. 2. Cambridge University Press.
[31] Ehret, G., Bousquet, P., Pierangelo, C., Alpers, M., Millet, B., Abshire, B. J., Bovensmann, H., Burrows, P. J., Chevallier, F., Ciais, P., Crevoisier, C., Fix, A., Flamant, P., Frankenberg, C., Gibert, F., Heim, B., Heimann, M., Houweling, S., Hubberten, W. H., Jöckel, P., Law, K., Löw, A., Marshall, J., Agusti-Panareda, A., Payan, S., Prigent, C., Rairoux, P., Sachs, T., Scholze, M., & Wirth, M. (2017). 'MERLIN: A French-German Space Lidar Mission Dedicated to Atmospheric Methane'. *Remote Sensing*, 9(10).

Table 2. GHG Emission Detection by Spaceborne Instruments

This table presents a summary of the types of GHG emissions that can be detected by current and future spaceborne instruments.

	Current Instruments					Future Instruments			
	Instrument Name	**Launch**	**Point Source Detection**	**Satellite Type**		**Instrument Name**	**Launch**	**Point Source Detection**	**Satellite Type**
XCO_2	AIRS	2002	No	Public	XCO_2	GOSAT-2	2018	No	Public
	IASI	2007	No	Public		CarbonSat	2020	Yes	Public
	GOSAT	2009	No	Public		IASI-NG	2021	No	Public
	OCO-2	2014	Partly	Public		geoCARB	2020 - 2023	No	Public
	TanSat	2016	No	Public		GeoFTS	proposed	No	Public
						G3E	proposed	Yes	Public
XCO	AIRS	2002	No	Public	XCO	GOSAT-2	2018	No	Public
	TROPOMI	2017	Partly	Public		Sentinel-5/UVNS	2021	No	Public
						geoCARB	2020 - 2023	No	Public
						GeoFTS	proposed	No	Public
						G3E	proposed	Yes	Public
XCH_4	AIRS	2002	No	Public	XCH_4	GOSAT-2	2018	No	Public
	IASI	2007	No	Public		Bluefield	2019 - 21	Yes	Private
	GOSAT	2009	No	Public		CarbonSat	2020	Yes	Public
	CrIS	2011	No	Public		Sentinel-5/UVNS	2021	No	Public
	GHGSat	2016	Yes	Private		geoCARB	2020 - 2023	No	Public
	TROPOMI	2017	Partly	Public		IASI-NG	2021	No	Public
						MERLIN	2021/22	Yes	Public
						GEO-CAPE	2022	Yes	Public
						GeoFTS	proposed	No	Public
						G3E	proposed	Yes	Public
XSO_2	AIRS	2002	No	Public	XSO_2	Sentinel-4/UVN	2019	No	Public
						Sentinel-5/UVNS	2021	No	Public
						GEO-CAPE	2022	Yes	Public
XNO_2					XNO_2	Sentinel-4/UVN	2019	No	Public
XNH_3					XNH_3	GEO-CAPE	2022	Yes	Public
XHCHO					XHCHO	Sentinel-4/UVN	2019	No	Public
						GEO-CAPE	2022	Yes	Public
XO_3	AIRS	2002	No	Public	XO_3	Sentinel-4/UVN	2019	No	Public
	IASI	2007	No	Public		Sentinel-5/UVNS	2021	No	Public
						IASI-NG	2021	No	Public

track nadir but some instruments also measure cross-track in the off-nadir that increases the spatial coverage. The characteristic absorption features of CH_4 are located in the shortwave infrared (SWIR) around 1650 and 2300 nm, and in the thermal infrared (TIR) at 8000 nm.[32] CO_2 can be derived in wavelength regions around 760, 1610 and 2060 nm.[33] Measurements in the SWIR are more sensitive to the near-surface atmospheric layers where the emitting sources are located, whereas TIR measurements provide a more regular sampling of the entire atmospheric column. This makes TIR retrievals less sensitive to CO_2 and CH_4 emissions local and regional scales.[34]

Table 2 provides an overview of the types of atmospheric GHG concentrations that can be measured by current and future spaceborne instruments. This table provides an indication of whether the instrument can be used to pinpoint emissions to a particular point source. Appendix A presents a more detailed overview of these satellites and their specifications. The Greenhouse Gases Observing Satellite (GOSAT) launched in 2009 measures at 1650 nm with high spectral resolution for CH_4 retrieval on a continental or regional scale of 100 to 1000 km.[35] It only measures at predefined pixel locations, which are partly separated by more than 250 km, leading to spatial observation gaps. It is also designed to deliver CO_2 concentrations using the 2060 nm fitting window.[36] In 2018 GOSAT-2 is planned to be launched, which will have higher precision and the ability to also detect CH_4 in the 2300 nm window.[37] The Tropospheric Monitoring Instrument (TROPOMI) launched in 2017 onboard the Sentinel-5p satellite is supposed to quantify daily emissions of CH_4 with the possibility to detect large point sources using the 2300 nm absorption feature. It simultaneously retrieves CO column concentration and provides a global coverage with a pixel resolution of 7 x 7 km^2.[38, 39, 40]

Furthermore, the European Space Agency (ESA) is preparing the UVNS instrument onboard Sentinel-5 to be launched in 2021.[41] Mentionable instruments for CO_2 monitoring in the SWIR region are the Orbiting Carbon Observatory 2 (OCO-2) measuring with a spatial resolution of max. 1.29 x 2.25 km^2, and the Carbon Dioxide Spectrometer (CDS) onboard the Chinese Carbon Dioxide Observation Satellite (TanSat) having a ground sampling distance of 1 x 2 km^2 and a 16-day revisiting time.[42, 43, 44] However, OCO-2 is not a mapping mission but a global sampling mission, which leads to wide spatial and temporal gaps

[32] Jacob, D. J., Turner, A. J., Maasakkers, J. D., Sheng, J., Sun, K., Liu, X., Chance, K., Aben, I., McKeever, J., & Frankenberg, C. (2016). 'Satellite observations of atmospheric methane and their value for quantifying methane emissions'. *Atmospheric Chemistry and Physics,* 16(22), 14371-14396.

[33] Nassar, R., Hill, T. G., McLinden, C. A., Wunch, D., Jones, D. B. A., & Crisp, D. (2017). 'Quantifying CO2 Emissions From Individual Power Plants From Space'. *Geophysical Research Letters,* 44(19), 10,045-10,053.

[34] Jacob, D. J., Turner, A. J., Maasakkers, J. D., Sheng, J., Sun, K., Liu, X., Chance, K., Aben, I., McKeever, J., & Frankenberg, C. (2016). 'Satellite observations of atmospheric methane and their value for quantifying methane emissions'. *Atmospheric Chemistry and Physics,* 16(22), 14371-14396.

[35] Kuze, A., Suto, H., Shiomi, K., Kawakami, S., Tanaka, M., Ueda, Y., Deguchi, A., Yoshida, J., Yamamoto, Y., & Kataoka, F. (2016). 'Update on GOSAT TANSO-FTS performance, operations, and data products after more than 6 years in space'. *Atmospheric Measurement Techniques,* 9(6).

[36] Nassar, R., Hill, T. G., McLinden, C. A., Wunch, D., Jones, D. B. A., & Crisp, D. (2017). 'Quantifying CO2 Emissions From Individual Power Plants From Space'. *Geophysical Research Letters,* 44(19), 10,045-10,053.

[37] Jacob, D. J., Turner, A. J., Maasakkers, J. D., Sheng, J., Sun, K., Liu, X., Chance, K., Aben, I., McKeever, J., & Frankenberg, C. (2016). 'Satellite observations of atmospheric methane and their value for quantifying methane emissions'. *Atmospheric Chemistry and Physics,* 16(22), 14371-14396.

[38] Butz, A., Galli, A., Hasekamp, O., Landgraf, J., Tol, P., & Aben, I. (2012). 'TROPOMI aboard Sentinel-5 Precursor: Prospective performance of CH4 retrievals for aerosol and cirrus loaded atmospheres'. *Remote Sensing of Environment,* 120(Supplement C), 267-276.

[39] Veefkind, J. P., Aben, I., McMullan, K., Förster, H., de Vries, J., Otter, G., Claas, J., Eskes, H. J., de Haan, J. F., Kleipool, Q., van Weele, M., Hasekamp, O., Hoogeveen, R., Landgraf, J., Snel, R., Tol, P., Ingmann, P., Voors, R., Kruizinga, B., Vink, R., Visser, H., & Levelt, P. F. (2012). 'TROPOMI on the ESA Sentinel-5 Precursor: A GMES mission for global observations of the atmospheric composition for climate, air quality and ozone layer applications'. *Remote Sensing of Environment,* 120(Supplement C), 70-83.

[40] Hu, H., Hasekamp, O., Butz, A., Galli, A., Landgraf, J., de Brugh, J. A., Borsdorff, T., Scheepmaker, R., & Aben, I. (2016). 'The operational methane retrieval algorithm for TROPOMI'. *Atmospheric Measurement Techniques,* 9(11), 5423.

[41] Ehret, G., Bousquet, P., Pierangelo, C., Alpers, M., Millet, B., Abshire, B. J., Bovensmann, H., Burrows, P. J., Chevallier, F., Ciais, P., Crevoisier, C., Fix, A., Flamant, P., Frankenberg, C., Gibert, F., Heim, B., Heimann, M., Houweling, S., Hubberten, W. H., Jöckel, P., Law, K., Löw, A., Marshall, J., Agusti-Panareda, A., Payan, S., Prigent, C., Rairoux, P., Sachs, T., Scholze, M., & Wirth, M. (2017). 'MERLIN: A French-German Space Lidar Mission Dedicated to Atmospheric Methane'. *Remote Sensing,* 9(10).

[42] Crisp, D., Pollock, H. R., Rosenberg, R., Chapsky, L., Lee, R. A., Oyafuso, F. A., Frankenberg, C., O'Dell, C. W., Bruegge, C. J., & Doran, G. B. (2017). 'The on-orbit performance of the Orbiting Carbon Observatory-2 (OCO-2) instrument and its radiometrically calibrated products'. *Atmospheric Measurement Techniques,* 10(1), 59.

[43] Nassar, R., Hill, T. G., McLinden, C. A., Wunch, D., Jones, D. B. A., & Crisp, D. (2017). 'Quantifying CO2 Emissions From Individual Power Plants From Space'. *Geophysical Research Letters,* 44(19), 10,045-10,053.

[44] Chen, X., Wang, J., Liu, Y., Xu, X., Cai, Z., Yang, D., Yan, C.-X., & Feng, L. (2017). 'Angular dependence of aerosol information content in CAPI/TanSat observation over land: Effect of polarization and synergy with A-train satellites'. *Remote Sensing of Environment,* 196, 163-177.

between the observations.[45] The commercial satellite GHGSat has a high spatial resolution of 50 x 50 m^2 and is therefore able to detect small point sources. However, it only covers selected observing targets and has a revisiting time of two weeks.[46] An even higher spatial resolution of 20 x 20 m^2 will be provided by the commercial Bluefield instruments. This constellation of microsatellites is scheduled to be in orbit from 2019 on, having a short revisiting time and global coverage for the monitoring of CH_4 emissions.[47] Another future instrument is the CarbonSat Satellite, which should provide CO_2 and CH_4 concentrations on a global scale with a spatial resolution of 2 x 2 km^2 leading to the ability to detect emission point sources.[48] Even hyperspectral instruments like the planned EnMAP mission, which is primarily not designed for GHG observation, have the potential to accurately detect emissions from point sources.[49] This assumption is based on a study[50] that found that the hyperspectral Hyperion sensor was able to detect CH_4 emissions from a single anthropogenic superemitter with a spatial resolution of 30m. In the field of lidar measurements the CH_4 Remote Sensing Lidar Mission (MERLIN) will be launched in 2021 or 2022 and monitor CH_4 emissions around 1650 nm by recording the along-track laser-emitted radiation reflected by the surface.[51, 52] It will provide data on a 0.15 x 0.15 km^2 grid with a revisiting time of 28 days.[53] Furthermore, new geostationary sensors will be launched in the future, including GEO-CAPE, GeoFTS, geoCARB (launch date after 2020) and G3E, which will measure at a continental scale with spatial resolutions between 375 m and 10 km.[54, 55, 56, 57, 58] In 2019, ESA and the European Organization for the Exploitation of Meteorological Satellites (EUMETSAT) plan to also launch a geostationary satellite (Meteosat Third Generation) carrying the Sentinel-4/UVN instrument with a spatial resolution of 8 x 8 km^2. It will be designed for the monitoring of O_3, NO_2, SO_2 and HCHO, however it will not be capable of

[45] Nassar, R., Hill, T. G., McLinden, C. A., Wunch, D., Jones, D. B. A., & Crisp, D. (2017). 'Quantifying CO2 Emissions From Individual Power Plants From Space'. *Geophysical Research Letters,* 44(19), 10,045-10,053.

[46] Jacob, D. J., Turner, A. J., Maasakkers, J. D., Sheng, J., Sun, K., Liu, X., Chance, K., Aben, I., McKeever, J., & Frankenberg, C. (2016). 'Satellite observations of atmospheric methane and their value for quantifying methane emissions'. *Atmospheric Chemistry and Physics,* 16(22), 14371-14396.

[47] Ariel, Y.(2017) Tracking methane emissions by using micro-satellites, available online:https://www.linkedin.com/pulse/tracking-methane-emissions-using-micro-satellites-yotam-ariel, accessed on 25 January 2018.

[48] Buchwitz, M., Reuter, M., Bovensmann, H., Pillai, D., Heymann, J., Schneising, O., Rozanov, V., Krings, T., Burrows, J., & Boesch, H. (2013). 'Carbon Monitoring Satellite (CarbonSat): assessment of scattering related atmospheric CO2 and CH4 retrieval errors and first results on implications for inferring city CO2 emissions'. *Atmospheric Measurement Techniques,* 6(12), 3477-3500.

[49] Guanter, L., Kaufmann, H., Segl, K., Foerster, S., Rogass, C., Chabrillat, S., Kuester, T., Hollstein, A., Rossner, G., Chlebek, C., Straif, C., Fischer, S., Schrader, S., Storch, T., Heiden, U., Mueller, A., Bachmann, M., Mühle, H., Müller, R., Habermeyer, M., Ohndorf, A., Hill, J., Buddenbaum, H., Hostert, P., van der Linden, S., Leitão, J. P., Rabe, A., Doerffer, R., Krasemann, H., Xi, H., Mauser, W., Hank, T., Locherer, M., Rast, M., Staenz, K., & Sang, B. (2015). 'The EnMAP Spaceborne Imaging Spectroscopy Mission for Earth Observation'. *Remote Sensing,* 7(7).

[50] Thompson, D. R., Thorpe, A. K., Frankenberg, C., Green, R. O., Duren, R., Guanter, L., Hollstein, A., Middleton, E., Ong, L., & Ungar, S. (2016). 'Space-based remote imaging spectroscopy of the Aliso Canyon CH4 superemitter'. *Geophysical Research Letters,* 43(12), 6571-6578.

[51] Kiemle, C., Quatrevalet, M., Ehret, G., Amediek, A., Fix, A., & Wirth, M. (2011). 'Sensitivity studies for a space-based methane lidar mission'. *Atmospheric Measurement Techniques,* 4(10), 2195.

[52] Ehret, G., Bousquet, P., Pierangelo, C., Alpers, M., Millet, B., Abshire, B. J., Bovensmann, H., Burrows, P. J., Chevallier, F., Ciais, P., Crevoisier, C., Fix, A., Flamant, P., Frankenberg, C., Gibert, F., Heim, B., Heimann, M., Houweling, S., Hubberten, W. H., Jöckel, P., Law, K., Löw, A., Marshall, J., Agusti-Panareda, A., Payan, S., Prigent, C., Rairoux, P., Sachs, T., Scholze, M., & Wirth, M. (2017). 'MERLIN: A French-German Space Lidar Mission Dedicated to Atmospheric Methane'. *Remote Sensing,* 9(10).

[53] Ehret, G., Bousquet, P., Pierangelo, C., Alpers, M., Millet, B., Abshire, B. J., Bovensmann, H., Burrows, P. J., Chevallier, F., Ciais, P., Crevoisier, C., Fix, A., Flamant, P., Frankenberg, C., Gibert, F., Heim, B., Heimann, M., Houweling, S., Hubberten, W. H., Jöckel, P., Law, K., Löw, A., Marshall, J., Agusti-Panareda, A., Payan, S., Prigent, C., Rairoux, P., Sachs, T., Scholze, M., & Wirth, M. (2017). 'MERLIN: A French-German Space Lidar Mission Dedicated to Atmospheric Methane'. *Remote Sensing,* 9(10).

[54] Fishman, J., Iraci, L. T., Al-Saadi, J., Chance, K., Chavez, F., Chin, M., Coble, P., Davis, C., DiGiacomo, P. M., Edwards, D., Eldering, A., Goes, J., Herman, J., Hu, C., Jacob, D. J., Jordan, C., Kawa, S. R., Key, R., Liu, X., Lohrenz, S., Mannino, A., Natraj, V., Neil, D., Neu, J., Newchurch, M., Pickering, K., Salisbury, J., Sosik, H., Subramaniam, A., Tzortziou, M., Wang, J., & Wang, M. (2012). 'The United States' Next Generation of Atmospheric Composition and Coastal Ecosystem Measurements: NASA's Geostationary Coastal and Air Pollution Events (GEO-CAPE) Mission'. *Bulletin of the American Meteorological Society,* 93(10), 1547-1566.

[55] Xi, X., Natraj, V., Shia, R.-L., Luo, M., Zhang, Q., Newman, S., Sander, S., & Yung, Y. (2015). 'Simulated retrievals for the remote sensing of CO 2, CH 4, CO, and H 2 O from geostationary orbit'. *Atmospheric Measurement Techniques,* 8(11), 4817.

[56] Polonsky, I., O'Brien, D., Kumer, J., & O'Dell, C. (2014). 'Performance of a geostationary mission, geoCARB, to measure CO 2, CH 4 and CO column-averaged concentrations'. *Atmospheric Measurement Techniques,* 7(4), 959-981.

[57] Butz, A., Orphal, J., Checa-Garcia, R., Friedl-Vallon, F., von Clarmann, T., Bovensmann, H., Hasekamp, O., Landgraf, J., Knigge, T., & Weise, D. (2015). 'Geostationary Emission Explorer for Europe (G3E): mission concept and initial performance assessment'. *Atmospheric Measurement Techniques,* 8(11), 4719.

[58] O'Brien, D. M., Polonsky, I. N., Utembe, S. R., & Rayner, P. J. (2016). 'Potential of a geostationary geoCARB mission to estimate surface emissions of CO 2, CH 4 and CO in a polluted urban environment: case study Shanghai'. *Atmospheric Measurement Techniques,* 9(9), 4633.

monitoring CH_4 or CO_2.[59] Current instruments using the TIR absorption feature for the CO_2 and CH_4 retrieval include the Atmospheric Infrared Sounder (AIRS), the Infrared Atmospheric Sounding Interferometer (IASI), and the Cross-track Infrared Sounder (CrIS).[60] Furthermore the French center for space science (CNES), in cooperation with EUMETSAT, plans to launch the next generation IASA (IASI-NG) in 2021.[61]

3.1.1.2. Airborne Instruments

Another way to detect GHG emissions from point sources is through the use of airborne sensors. They basically use the same retrieval methods as spaceborne instruments but have distinct spatial resolution, at the expense of a much coarser spectral resolution. Examples are the Methane Airborne Mapper (MAMAP), the Next Generation Airborne Visible/Infrared Imaging Spectrometer (AVIRIS-NG), which is also able to derive CO_2 and water vapour concentrations, and the Hyperspectral Thermal Emission Spectrometer (HyTES).[62, 63, 64] The latter two instruments provide a detection threshold of 2 kg h^{-1}.[65] Using these sensors the plume structure can be observed in detail to better determine the source of emission. LIDAR instruments can also be used from airborne platforms to monitor CH_4 and CO_2. One example is the recently developed CHARM-F, which in several tests achieved a precision of better than 0.5%.[66] Furthermore, airborne instruments measuring in the TIR range can be used to detect CH_4 point sources. For example, the Spatially-Enhanced Broadband Array Spectrograph System (SEBASS) sensor has been proven to be suitable for refining CH_4 emission estimates.[67]

3.1.2. Retrieval Methods

Commonly, GHG retrievals in the SWIR operate by fitting a modelled reflectance spectrum to the one measured by the instrument. Normally physically-based models are used to simulate spectral reflectance or radiance as a function of illumination/observation geometry, surface reflectance and atmospheric composition. XCH_4 and XCO_2 are among the parameters in the model that are estimated through the fit. Parameters needed for this atmospheric inversion technique are the viewing geometry and a first guess of

[59] Bazalgette Courrèges-Lacoste, G., Ahlers, B., Guldimann, B., Short, A., Veihelmann, B., and Stark, H. (2018). 'The Sentinel-4/UVN instrument on-board MTG-S', ESA ESTEC, Nordwijk, The Netherlands.

[60] Jacob, D. J., Turner, A. J., Maasakkers, J. D., Sheng, J., Sun, K., Liu, X., Chance, K., Aben, I., McKeever, J., & Frankenberg, C. (2016). 'Satellite observations of atmospheric methane and their value for quantifying methane emissions'. *Atmospheric Chemistry and Physics,* 16(22), 14371-14396.

[61] Crevoisier, C., Clerbaux, C., Guidard, V., Phulpin, T., Armante, R., Barret, B., Camy-Peyret, C., Chaboureau, J.-P., Coheur, P.-F., Crépeau, L., Dufour, G., Labonnote, L., Lavanant, L., Hadji-Lazaro, J., Herbin, H., Jacquinet-Husson, N., Payan, S., Péquignot, E., Pierangelo, C., Sellitto, P., & Stubenrauch, C. (2014). 'Towards IASI-New Generation (IASI-NG): impact of improved spectral resolution and radiometric noise on the retrieval of thermodynamic, chemistry and climate variables'. *Atmospheric Measurement Techniques,* 7, 4367-4385.

[62] Gerilowski, K., Tretner, A., Krings, T., Buchwitz, M., Bertagnolio, P., Belemezov, F., Erzinger, J., Burrows, J., & Bovensmann, H. (2011). 'MAMAP-a new spectrometer system for column-averaged methane and carbon dioxide observations from aircraft: instrument description and performance analysis'. *Atmospheric Measurement Techniques,* 4(2), 215.

[63] Frankenberg, C., Thorpe, A. K., Thompson, D. R., Hulley, G., Kort, E. A., Vance, N., Borchardt, J., Krings, T., Gerilowski, K., Sweeney, C., Conley, S., Bue, B. D., Aubrey, A. D., Hook, S., & Green, R. O. (2016). 'Airborne methane remote measurements reveal heavy-tail flux distribution in Four Corners region'. *Proceedings of the National Academy of Sciences,* 113(35), 9734-9739.

[64] Thorpe, A. K., Frankenberg, C., Thompson, D. R., Duren, R. M., Aubrey, A. D., Bue, B. D., Green, R. O., Gerilowski, K., Krings, T., & Borchardt, J. (2017). 'Airborne DOAS retrievals of methane, carbon dioxide, and water vapor concentrations at high spatial resolution: application to AVIRIS-NG'. *Atmospheric Measurement Techniques,* 10(10), 3833.

[65] Thorpe, A. K., Frankenberg, C., Aubrey, A. D., Roberts, D. A., Nottrott, A. A., Rahn, T. A., Sauer, J. A., Dubey, M. K., Costigan, K. R., Arata, C., Steffke, A. M., Hills, S., Haselwimmer, C., Charlesworth, D., Funk, C. C., Green, R. O., Lundeen, S. R., Boardman, J. W., Eastwood, M. L., Sarture, C. M., Nolte, S. H., McCubbin, I. B., Thompson, D. R., & McFadden, J. P. (2016). 'Mapping methane concentrations from a controlled release experiment using the next generation airborne visible/infrared imaging spectrometer (AVIRIS-NG)'. *Remote Sensing of Environment,* 179, 104-115.

[66] Amediek, A., Ehret, G., Fix, A., Wirth, M., Büdenbender, C., Quatrevalet, M., Kiemle, C., & Gerbig, C. (2017). 'CHARM-F a new airborne integrated-path differential-absorption lidar for carbon dioxide and methane observations: measurement performance and quantification of strong point source emissions'. *Applied Optics,* 56(18), 5182-5197.

[67] Scafutto, R. D. M., de Souza Filho, C. R., Riley, D. N., & de Oliveira, W. J. (2018). 'Evaluation of thermal infrared hyperspectral imagery for the detection of onshore methane plumes: Significance for hydrocarbon exploration and monitoring'. *International Journal of Applied Earth Observation and Geoinformation,* 64, 311-325.

atmospheric state constituents.[68, 69] GOSAT and TROPOMI, for instance, use a full-physics method to fit the scattering properties of the surface and the atmosphere. In this context, full-physics means using additional parameters to fit the scattering by cirrus and aerosols utilising a preferably accurate radiative transfer model.[70, 71] OCO-2 uses a slightly different method by fitting the observed concentrations to those simulated by a Gaussian plume model.[72] MERLIN uses the integrated path differential absorption (IPDA) technique based on differential absorption lidar (DIAL) where two different frequencies are exploited, one to be the reference with only weak CH_4 absorption and the other to represent the spectral feature.[73]

3.1.3. Detection Thresholds and Retrieval Precision

According to their specifications, the commercial instruments GHGSat and Bluefield are able to detect CH_4 emissions down to 0.24 t h^{-1} and even 0.015 t h^{-1}, respectively, which is the lowest detection threshold of all considered instruments.[74, 75] GOSAT has a limit of 7.1 t h^{-1} that will be enhanced by GOSAT-2 with a limit of 4.0 t h^{-1}. TROPOMI detects point sources as small as 4.2 t h^{-1}, whereas CarbonSat's threshold for a single pixel will be 0.8 t h^{-1}. The future geostationary sensors predominantly feature low detection thresholds of 4.0 t h^{-1} for GEO-CAPE and geoCARB, 1.3 t h^{-1} for G3E, and 0.61 t h^{-1} for GeoFTS. The threshold for MERLIN has not yet been estimated.[76]

Generally, the retrieval precision for CH_4 has to be better than 2% in order to identify enhancements caused by emissions above the atmospheric background concentration of around 1800 ppb.[77] The World Meteorological Organization (WMO) even recommends a precision better than 0.1%. For CO_2 retrievals the precision should be at least 4000 ppb to enable an accurate quantification.[78, 79] The presence of clouds strongly affects the retrieval, so all instruments seek to exclude cloudy scenes. GOSAT uses a simultaneous O_2 retrieval at 760 nm since a low oxygen column suggests a clouded pixel. This leads to a

[68] Frankenberg, C., Meirink, J. F., Bergamaschi, P., Goede, A. P. H., Heimann, M., Körner, S., Platt, U., van Weele, M., & Wagner, T. (2006). 'Satellite chartography of atmospheric methane from SCIAMACHY on board ENVISAT: Analysis of the years 2003 and 2004'. *Journal of Geophysical Research: Atmospheres,* 111(D7).

[69] Schepers, D., Guerlet, S., Butz, A., Landgraf, J., Frankenberg, C., Hasekamp, O., Blavier, J. F., Deutscher, N. M., Griffith, D. W. T., Hase, F., Kyro, E., Morino, I., Sherlock, V., Sussmann, R., & Aben, I. (2012). 'Methane retrievals from Greenhouse Gases Observing Satellite (GOSAT) shortwave infrared measurements: Performance comparison of proxy and physics retrieval algorithms'. *Journal of Geophysical Research: Atmospheres,* 117(D10).

[70] Jacob, D. J., Turner, A. J., Maasakkers, J. D., Sheng, J., Sun, K., Liu, X., Chance, K., Aben, I., McKeever, J., & Frankenberg, C. (2016). 'Satellite observations of atmospheric methane and their value for quantifying methane emissions'. *Atmospheric Chemistry and Physics,* 16(22), 14371-14396.

[71] Ehret, G., Bousquet, P., Pierangelo, C., Alpers, M., Millet, B., Abshire, B. J., Bovensmann, H., Burrows, P. J., Chevallier, F., Ciais, P., Crevoisier, C., Fix, A., Flamant, P., Frankenberg, C., Gibert, F., Heim, B., Heimann, M., Houweling, S., Hubberten, W. H., Jöckel, P., Law, K., Löw, A., Marshall, J., Agusti-Panareda, A., Payan, S., Prigent, C., Rairoux, P., Sachs, T., Scholze, M., & Wirth, M. (2017). 'MERLIN: A French-German Space Lidar Mission Dedicated to Atmospheric Methane'. *Remote Sensing,* 9(10).

[72] Nassar, R., Hill, T. G., McLinden, C. A., Wunch, D., Jones, D. B. A., & Crisp, D. (2017). 'Quantifying CO2 Emissions From Individual Power Plants From Space'. *Geophysical Research Letters,* 44(19), 10,045-10,053.

[73] Ehret, G., Bousquet, P., Pierangelo, C., Alpers, M., Millet, B., Abshire, B. J., Bovensmann, H., Burrows, P. J., Chevallier, F., Ciais, P., Crevoisier, C., Fix, A., Flamant, P., Frankenberg, C., Gibert, F., Heim, B., Heimann, M., Houweling, S., Hubberten, W. H., Jöckel, P., Law, K., Löw, A., Marshall, J., Agusti-Panareda, A., Payan, S., Prigent, C., Rairoux, P., Sachs, T., Scholze, M., & Wirth, M. (2017). 'MERLIN: A French-German Space Lidar Mission Dedicated to Atmospheric Methane'. *Remote Sensing,* 9(10).

[74] Jacob, D. J., Turner, A. J., Maasakkers, J. D., Sheng, J., Sun, K., Liu, X., Chance, K., Aben, I., McKeever, J., & Frankenberg, C. (2016). 'Satellite observations of atmospheric methane and their value for quantifying methane emissions'. *Atmospheric Chemistry and Physics,* 16(22), 14371-14396.

[75] Bluefield: Innovation, (2018). available online: http://bluefield.co/, accessed on 25 January 2018.

[76] Jacob, D. J., Turner, A. J., Maasakkers, J. D., Sheng, J., Sun, K., Liu, X., Chance, K., Aben, I., McKeever, J., & Frankenberg, C. (2016). 'Satellite observations of atmospheric methane and their value for quantifying methane emissions'. *Atmospheric Chemistry and Physics,* 16(22), 14371-14396.

[77] Ehret, G., Bousquet, P., Pierangelo, C., Alpers, M., Millet, B., Abshire, B. J., Bovensmann, H., Burrows, P. J., Chevallier, F., Ciais, P., Crevoisier, C., Fix, A., Flamant, P., Frankenberg, C., Gibert, F., Heim, B., Heimann, M., Houweling, S., Hubberten, W. H., Jöckel, P., Law, K., Löw, A., Marshall, J., Agusti-Panareda, A., Payan, S., Prigent, C., Rairoux, P., Sachs, T., Scholze, M., & Wirth, M. (2017). 'MERLIN: A French-German Space Lidar Mission Dedicated to Atmospheric Methane'. *Remote Sensing,* 9(10).

[78] Miller, C. E., Crisp, D., DeCola, P. L., Olsen, S. C., Randerson, J. T., Michalak, A. M., Alkhaled, A., Rayner, P., Jacob, D. J., Suntharalingam, P., Jones, D. B. A., Denning, A. S., Nicholls, M. E., Doney, S. C., Pawson, S., Boesch, H., Connor, B. J., Fung, I. Y., O'Brien, D., Salawitch, R. J., Sander, S. P., Sen, B., Tans, P., Toon, G. C., Wennberg, P. O., Wofsy, S. C., Yung, Y. L., & Law, R. M. (2007). 'Precision requirements for space-based data'. *Journal of Geophysical Research: Atmospheres,* 112(D10).

[79] Rayner, P. J., & O'Brien, D. M. (2001). 'The utility of remotely sensed CO2 concentration data in surface source inversions'. *Geophysical Research Letters,* 28(1), 175-178.

ratio of 17% of successful retrievals.[80] For a single GOSAT observation the precision of the CH_4 retrieval using the full-physics method is about 1%, whereas CO_2 is retrieved with a lower precision of 2%.[81] GOSAT-2 is expected to have a single retrieval precision of about 0.4% for CH_4.[82] The TROPOMI sensor applies observations from the Visible Infrared Imaging Radiometer Suite (VIIRS), which covers the same scenes in order to detect clouded pixels.[83] The retrieval can successfully be applied to more than 90% of observed cloud-free scenes with a precision better than 1%.[84] MERLIN provides a precision of 1-2% for global mapping of CH_4 concentrations on a 50 x 50 km² grid by monthly and spatial averaging.[85] This precision should be outperformed by CarbonSat with a designated precision of 0.4%.[86] Finally, the TIR instrument IASI has a precision of about 1.2%.[87]

3.1.4. Conclusion

The few currently existing spaceborne instruments have several limitations. GOSAT provides retrieval products of high quality but has wide spatial observation gaps and a pixel size not below 10 km. TROPOMI is only able to detect large point sources and cannot be used for measuring GHG emissions at the asset-level. Figure 1 presents an overview of the launch dates plotted against the ground sampling distance for the most relevant GHG measuring instruments. The most suitable instruments, which are below the necessary detection threshold, are GHGSat, Bluefield and CarbonSat. They are all able to resolve individual plumes, with Bluefield having the highest potential due to a spatial resolution of 20 x 20 m². However, GHGSat and Bluefield are commercial satellites and their data products are not freely accessible and both Bluefield and the CarbonSat instrument are not yet launched. Furthermore, monitoring GHG emissions from space is always limited by the accuracy of the applied radiative transfer model and by the data availability in space and time. Active instruments like MERLIN have the advantage of being independent from solar radiation and cloud cover and are thus able to measure during all seasons, at all latitudes, and during day and night.[88] On the other hand, the sensor will not be launched until 2021 and has a comparably long revisiting time of 28 days. Overall, the direct method of emission monitoring is currently feasible for a relatively limited scope of assets (such as assets that are situated in regions with very few other sources of emissions in the surrounding area). However, the launch of the CarbonSat satellite in 2020 as well as some already scheduled sun-synchronous sensors offer the potential for more precise observation of GHG concentrations and emissions at the asset-level.

[80] Parker, R., Boesch, H., Cogan, A., Fraser, A., Feng, L., Palmer, P. I., Messerschmidt, J., Deutscher, N., Griffith, D. W. T., Notholt, J., Wennberg, P. O., & Wunch, D. (2011). 'Methane observations from the Greenhouse Gases Observing SATellite: Comparison to ground-based TCCON data and model calculations'. *Geophysical Research Letters,* 38(15).

[81] Kuze, A., Suto, H., Shiomi, K., Kawakami, S., Tanaka, M., Ueda, Y., Deguchi, A., Yoshida, J., Yamamoto, Y., & Kataoka, F. (2016). 'Update on GOSAT TANSO-FTS performance, operations, and data products after more than 6 years in space'. *Atmospheric Measurement Techniques,* 9(6).

[82] Jacob, D. J., Turner, A. J., Maasakkers, J. D., Sheng, J., Sun, K., Liu, X., Chance, K., Aben, I., McKeever, J., & Frankenberg, C. (2016). 'Satellite observations of atmospheric methane and their value for quantifying methane emissions'. *Atmospheric Chemistry and Physics,* 16(22), 14371-14396.

[83] Veefkind, J. P., Aben, I., McMullan, K., Förster, H., de Vries, J., Otter, G., Claas, J., Eskes, H. J., de Haan, J. F., Kleipool, Q., van Weele, M., Hasekamp, O., Hoogeveen, R., Landgraf, J., Snel, R., Tol, P., Ingmann, P., Voors, R., Kruizinga, B., Vink, R., Visser, H., & Levelt, P. F. (2012). 'TROPOMI on the ESA Sentinel-5 Precursor: A GMES mission for global observations of the atmospheric composition for climate, air quality and ozone layer applications'. *Remote Sensing of Environment,* 120(Supplement C), 70-83.

[84] Butz, A., Galli, A., Hasekamp, O., Landgraf, J., Tol, P., & Aben, I. (2012). 'TROPOMI aboard Sentinel-5 Precursor: Prospective performance of CH4 retrievals for aerosol and cirrus loaded atmospheres'. *Remote Sensing of Environment,* 120(Supplement C), 267-276.

[85] Kiemle, C., Quatrevalet, M., Ehret, G., Amediek, A., Fix, A., & Wirth, M. (2011). 'Sensitivity studies for a space-based methane lidar mission'. *Atmospheric Measurement Techniques,* 4(10), 2195.

[86] Jacob, D. J., Turner, A. J., Maasakkers, J. D., Sheng, J., Sun, K., Liu, X., Chance, K., Aben, I., McKeever, J., & Frankenberg, C. (2016). 'Satellite observations of atmospheric methane and their value for quantifying methane emissions'. *Atmospheric Chemistry and Physics,* 16(22), 14371-14396.

[87] Crevoisier, C., Nobileau, D., Armante, R., Crépeau, L., Machida, T., Sawa, Y., Matsueda, H., Schuck, T., Thonat, T., & Pernin, J. (2013). 'The 2007–2011 evolution of tropical methane in the mid-troposphere as seen from space by MetOp-A/IASI'. *Atmospheric Chemistry and Physics,* 13(8), 4279-4289.

[88] Ehret, G., Bousquet, P., Pierangelo, C., Alpers, M., Millet, B., Abshire, B. J., Bovensmann, H., Burrows, P. J., Chevallier, F., Ciais, P., Crevoisier, C., Fix, A., Flamant, P., Frankenberg, C., Gibert, F., Heim, B., Heimann, M., Houweling, S., Hubberten, W. H., Jöckel, P., Law, K., Löw, A., Marshall, J., Agusti-Panareda, A., Payan, S., Prigent, C., Rairoux, P., Sachs, T., Scholze, M., & Wirth, M. (2017). 'MERLIN: A French-German Space Lidar Mission Dedicated to Atmospheric Methane'. *Remote Sensing,* 9(10).

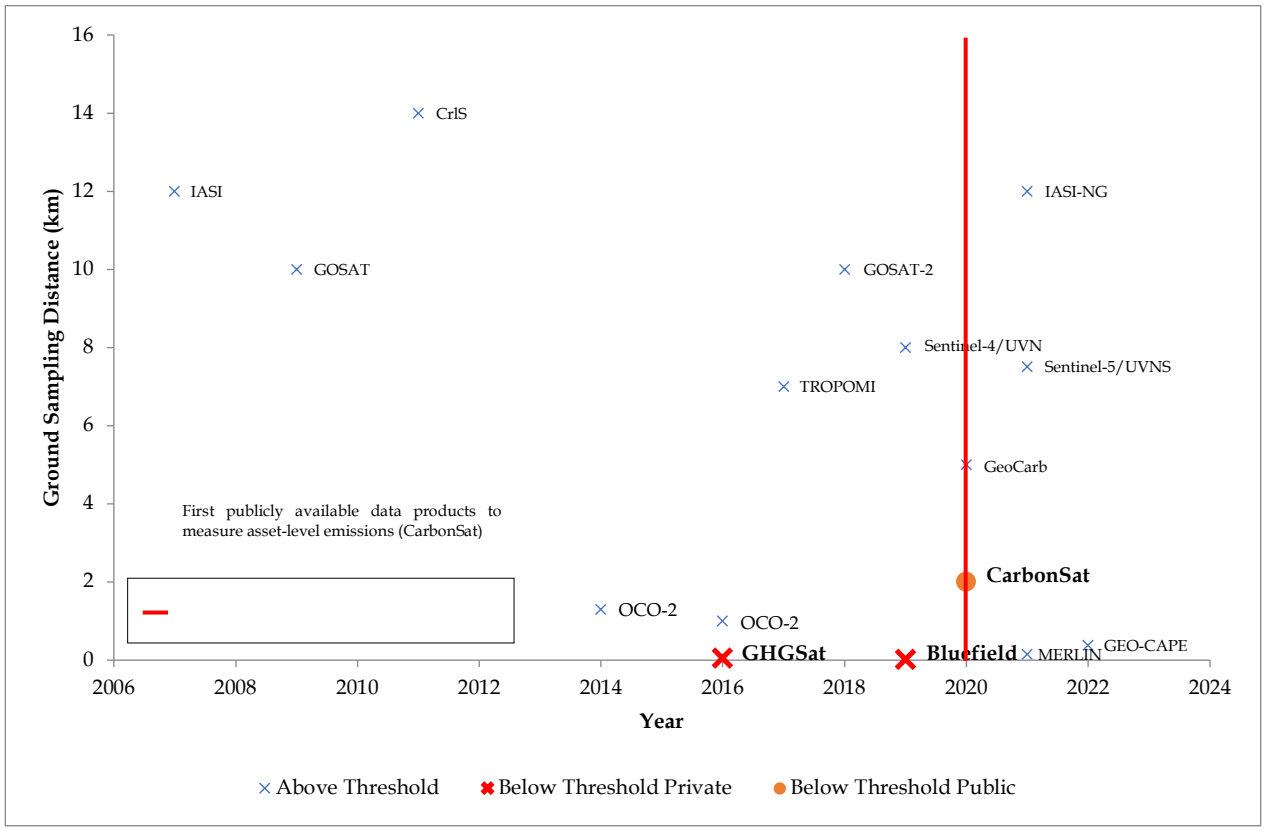

Figure 1: Launch Dates of Current and Future GHG Satellite Missions
This figure plots the launch date against the ground sampling distance of all major GHG measuring satellites. Satellites are defined as below threshold if the detection threshold is below 1 th^{-1}, which is sufficient for the identification of emissions to a particular asset.

3.2. Indirect Emissions Monitoring

The direct method of measuring GHG concentrations through spaceborne and airborne instruments is one possible way of monitoring emissions from assets. An alternative approach is to model GHG emissions indirectly using identifiable asset characteristics.

The indirect methodology first requires the identification of key characteristics that are associated with GHG emissions. For example asset utilisation rates are inherently linked to the level of GHG emissions. Using some of the spaceborne instruments in combination with real asset-level production data[89] it is possible to model temporal variations in an asset's utilisation rate. Employing this projection of the utilisation rate an estimate of the emissions can then be obtained using a standardised model, such as those outlined in the IPCC guidelines.

The most notable drawbacks of the direct methods are the relatively low resolution of current instruments and the imprecise nature of the retrieval methods. This method while still having its own drawbacks avoids these limitations associated with the direct method. The main drawbacks of the indirect approach are the ability to effectively identify asset characteristics and the accuracy of the modelling of the GHG emissions. Despite these potential impediments the indirect approach represents a more feasible methodology of emissions measurements based on currently available technology.

[89] For example see https://www.eex-transparency.com

4. Asset Environment and Localisation

Asset localisation refers to the determination of the precise geospatial footprint of a physical asset. For many asset classes, asset-level datasets are only weakly localised (e.g. to the closest town), adding a layer of proximity error between the asset of interest and the environmental risk being assessed. Environmental risk is inherently geospatial and is heterogeneous across scales – e.g. the geospatial scale required to assess risk exposure to protected areas or habitats is different to the scale required to assess chronic flood/drought risk exposure. The precise localisation of assets is required to avoid propagating scale errors for various risk metrics.

Further, for many asset classes, a satisfactory public data set of real economy assets does not exist. Such datasets are prerequisite to analyses of environmental risk. Asset localisation offers a method to synthetically derive these datasets by identifying asset footprints in remote sensing imagery. Training data can be developed from 'seed' data of known assets. This also offers a method for completing datasets with large regional gaps.

The environment an asset is located in is an important heuristical input to the detection of physical assets. Coal mines, for example, are unlikely to be in built-up urban centres. Farms are unlikely to be located in arid deserts. Land use classification is a canonical problem in remote sensing applications. This section provides an overview of methods that can be used to identify the environment an asset is situated in as well as how current databases can be used to facilitate the classification of assets.

4.1. Automatic Asset Environment Classification

The specific environment of assets is of major importance for an adequate analysis and estimation of their vulnerability in relation to climate change. However, manual classification of environments is challenging and requires a substantial amount of operator time and effort. As information about asset locations are increasing rapidly, environment classification needs to be automated, in order to keep pace.

Two challenges need to be solved: The first is the automatic classification of the Earth's surface using satellite remote sensing data. This involves the selection of appropriate data (spatial/ spectral resolution/ coverage), the selection of appropriate algorithms to process the data, as well as the development of a classification scheme that fits the processed data – i.e. the observed land cover - into pre-defined categories. The second challenge is to develop a stable routine that extracts the required information about an asset of interest from the previously classified global land cover-type products.

Numerous studies and researchers developed algorithms and routines to classify land surfaces or objects in aerial and satellite images, based on their spectral response in multiple wavelengths (visible, UV, IR, etc.), starting in the 1950s.[90, 91] Based on this, several data products are already available, which offer global classification maps of the Earth's surface in high resolution and accuracy. As creation of such a global classification map is time consuming, an already existing map provided by the European Space Agency's (ESA) Climate Change Initiative (CCI) has been used for this study (Figure 2).[92] The map is actualised in regular time intervals (bi-annually) and provides information with a spatial resolution of 300m per pixel and 38 different classes, ranging from urban over forest to agricultural areas. As this variety of different classes is not required for the intention of this study, all classes were reduced to 7 final super-classes, namely urban, forest, grass, soil, snow & ice, cropland and coastal. Utilisation of the CCI map is free for research purposes, but can be requested for projects outside of academia as well.

The listed classes consist of several subclasses from the original ESA CCI classification map, for example the "cropland" class contains the original classes "mosaic cropland" and "cropland irrigated or post-flooding", and "cropland rainfed", while the class "soil" contains "bare areas", "consolidated bare areas", and "unconsolidated bare areas". This system is flexible, and specific classes can be included or excluded from the investigation, if required. In general, the 7 main classes facilitates the analysis of the global

[90] Marschner, F. J. (1950) Major land uses in the United States. *U.S. Department of Agriculture, Agr. Research Service*.
[91] Anderson, J. R., Hardy, E. E., Roach, J. T., & Witmer, R. E. (1976) A Land use and Land Cover Classification System for Use with Remote Sensor data. *Geological Survey Professional Paper 964*.
[92] ESA CCI. (2018) Land cover map viewer. URL: http://maps.elie.ucl.ac.be/CCI/viewer/ (Status: 11.04.18).

distribution of the most important asset environments: The occurrence of the coastal class in the vicinity of an asset allows us to identify whether a location is situated close to the sea, which is useful for an assessment of flood risk. In addition, by exploiting the information stored in the ESA CCI classification map, the relative distribution of specific classes around the globe - independent from specific assets - can be analysed, to measure the extent of cropland in a specific country. As an example of cropland identification, Figure 3 displays a scene in a part of southern Germany within ESA's CCI land cover map. Utilising the map's information, detailed studies about local, regional, and global cropland distribution can be performed. Unfortunately, differences between crop types are not recognised by the original classification scheme and can therefore not be extracted.

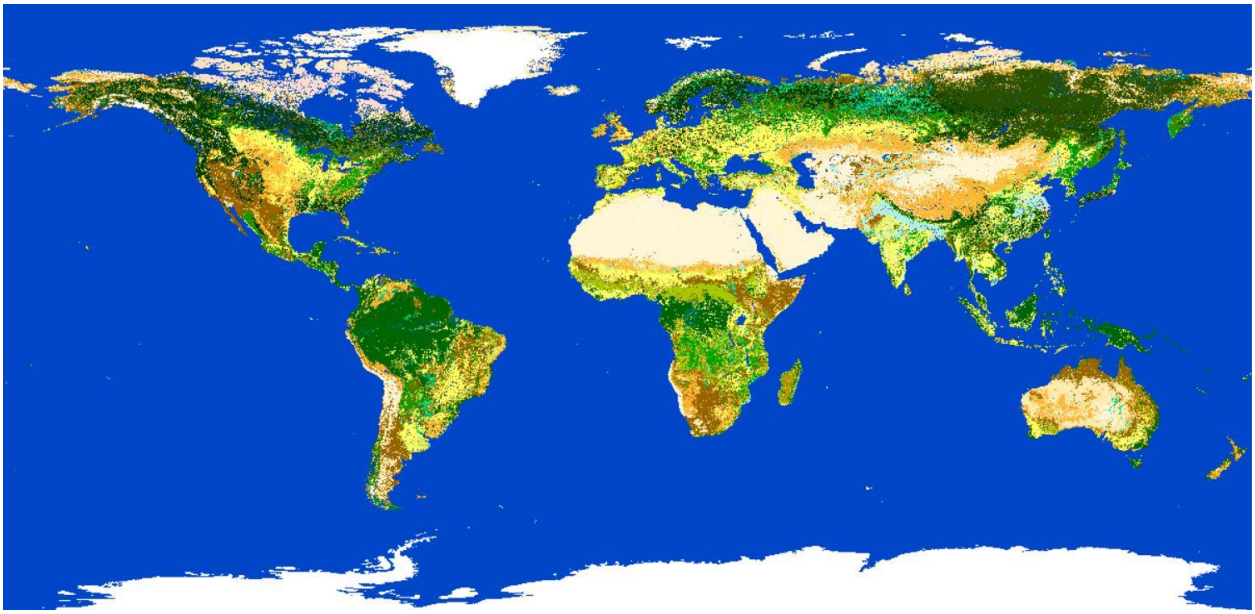

Figure 2: ESA CCI classification map
Colours represent the 38 different original classes (taken from ESA CCI, 2018).

As the ESA CCI map is regularly updated, the evolution and utilisation of land can be tracked over time caused by economic growth or even natural disasters. Further, the relative distribution of classes within a country can be analysed, for example whether the area covered by urban areas is increasing and which other classes are decreasing in turn.

With classification data on hand, the next step is to extract the information of the surrounding areas of an asset of interest. By using the asset's longitude and latitude, a circular extraction mask of previously specified dimensions can be fitted onto the map that contains the classification information. As the classification map is in a cartographic projection, the extraction mask's dimensions are connected to the latitude of the asset; a higher latitude generates a larger extraction mask, to account for projection-related errors. The circular shape of the mask allows an equally weighted extraction of all intra-mask pixels (i.e. pixels with the same distance from the asset), in contrast to a rectangular mask shape, which would extract pixels with different distances from the asset (from its corners), while giving weight to more distant and therefore less relevant pixels. Subsequently, the routine calculates the relative abundance of all classes within the mask and determines the most abundant class. This majority class is defined as the asset's environment.

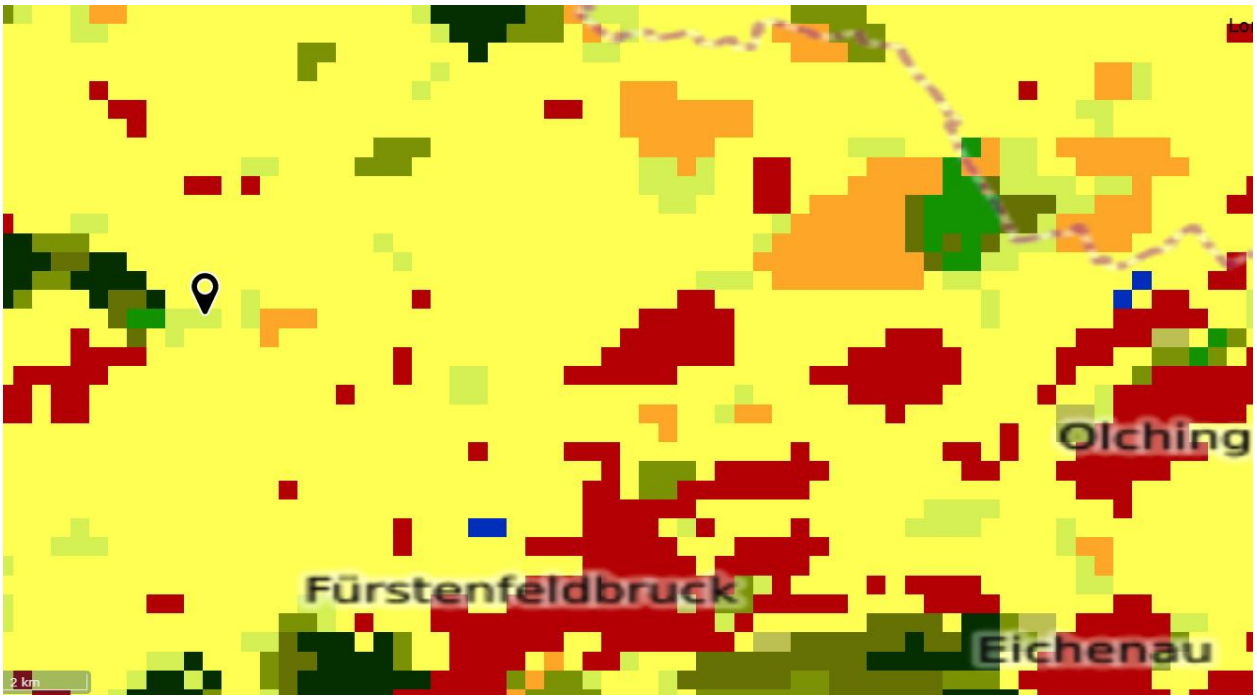

Figure 3: Scene from ESA's CCI land cover map in southern Germany, close to the cities Fürstenfeldbruck and Olching
Yellowish and light green colours indicate cropland areas ("cropland rainfed" and "mosaic cropland"), intermediate and dark green represent grassland or forest areas, red are urban areas; scene is ~25 km across, N is up (taken from ESA CCI, 2018).

As the environment of an asset differs depending on the scale of the extraction mask (cf. to Figure 4), the described extraction mask is applied three times, with a very small size (immediate surrounding), with an intermediate size (wider surrounding), and with a very large size (continental context). This cascading classification allows the recognition of an asset; that is situated in an urban area (1st mask, urban), that is surrounded by forest (2nd mask, forest), and that is close to the sea (3rd mask, coastal).

Limitations of this technique are on the one hand its dependency on the accuracy of the underlying ESA CCI classification map and on the other hand the assumption that the most abundant class within the extraction mask is representative of the asset's environment. Masks that contain two or more classes with very similar abundances (e.g. a mask with 51% forest and with 49% urban), might not be indicative of its environment (it is classified as forest only, although it is also urban to a significant extent). The cascading extraction masks attempt to account for this ambiguity but cannot completely resolve it. Despite its limitations, the application of this routine on existing data about asset locations provides an understanding of their environment and thus a better estimation of their vulnerability to climate change.

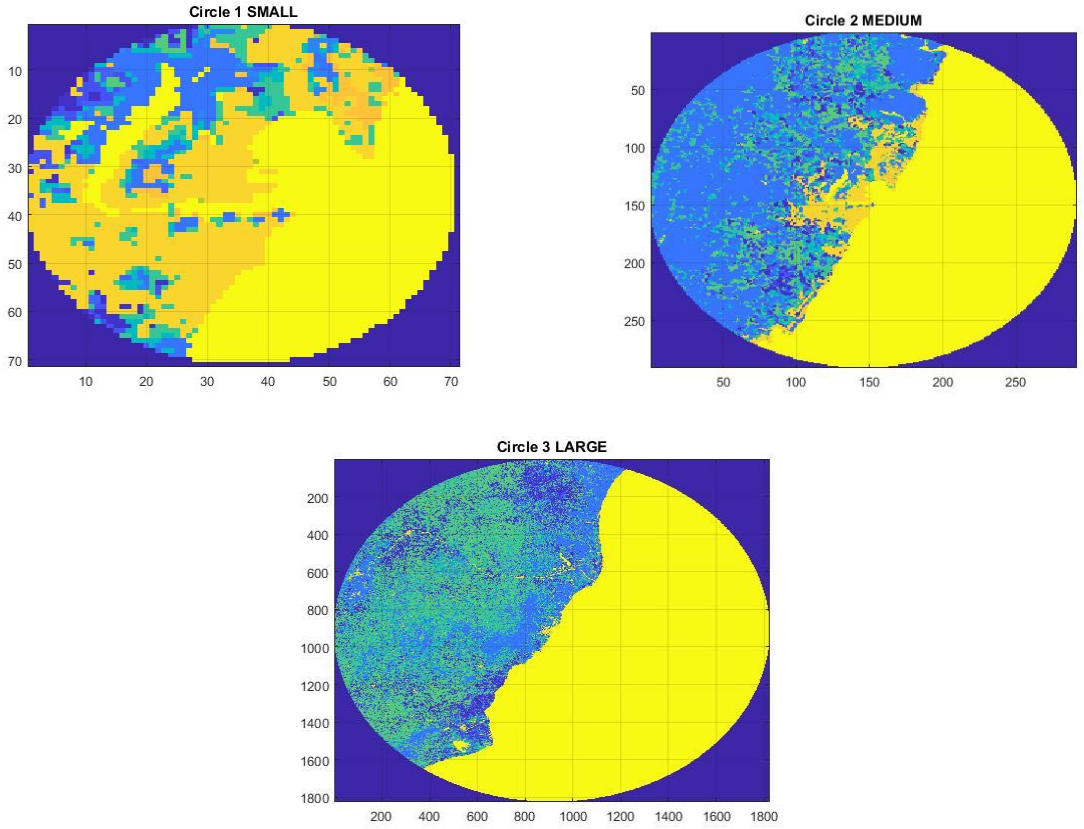

Figure 4: Example of a Small Extraction Mask
False-colour example of a small extraction mask (asset in Brazil), yellow represents water, orange represents urban, and blue and green represent forest areas. Top image, characterised by the urban class (in orange), second image, characterised by the forest class (in green and blue), and the bottom image, characterised by the coastal class (in yellow). All masks are placed on the ESA CCI land cover map for the extraction.

4.2. Utilisation of OpenStreetMap for Asset Identification and Localisation

The collection of reliable information about the location and type of assets on a global scale is difficult and time-consuming. In order to facilitate and speed up this process, existing databases could be exploited. OpenStreetMap is a platform which contains information about numerous objects, including data about locations and the extent of industrial areas.[93]

This information is saved within OpenStreetMap's database - or in connected databases such as OpenWhatEverMap[94] - either in vectorised form (polygons), including longitude and latitude as well as descriptive tags (such as industrial, agriculture, etc.) or as descriptive text strings (Figure 5). There are two possibilities to extract this information. First, an area of interest could be defined and all information within this area could be extracted. This could be useful to validate previously derived (e.g. by web crawling) latitude and longitude information and to check whether an identified location is actually a real asset or not. If the same asset is tagged or located at the same position in OpenStreetMap, it is probably real. On the other hand, the entire stack of vectorised data and text strings could be scanned (globally), while aiming for specific tags (tag/text search). Subsequently, the longitude and latitude information, which is connected to the respective tags of all found matches (e.g. all industrial areas) could be extracted and added to existing databases. At the same time, tagged polygons could be used to distinguish different assets (for example production sites from office sites), if the respective tags are available. Such a distinction might be impossible using optical/multispectral satellite imagery alone. Further,

[93] OSM. (2018) OpenStreetMap - About. URL: https://www.openstreetmap.org/about (Status: 11.4.18).
[94] OWEM. (2018) OpenWhatEverMap. URL: http://openwhatevermap.xyz/#3/28.00/18.00 (Status: 11.4.18).

OpenStreetMap contains other useful data, such as building heights or locations of public buildings. This additional information could be used for other aspects of climate risk analysis, such as susceptibility of high-rise buildings to winds.

Vectorised and geo-referenced information (polygons, lines, points) can be accessed using software such as QGIS. However, the extraction of information is limited by the fact that the distribution and availability of information is very heterogeneous and highly dependent on the location of the area of interest. Specific information might not be available in all countries or might vary in quality and reliability. This also underlines the fact that all extracted information requires sufficient (manual) validation, in order to enable a sophisticated estimate of the contained errors and uncertainties. However, OpenStreetMap is an ongoing project with a global community and the amount and quality of information is improving. For this reason, the exploitation of OpenStreetMap is particularly promising to expand existing databases, while improving their quality.

Figure 5: Example of an Asset in OpenStreetMap
Exemplary cut-out taken from OpenStreetMap of an asset in the UAE; mapped polygons with information are marked in green, the polygon tagged as "industrial" is highlighted in red (centre of the figure). A cross-check with optical imagery and available information from the web confirms that this is an industrial site.

5. Sectoral Details

This section provides a pilot study for several key industries to assess the feasibility of identifying types of assets and their features remotely. Throughout this pilot study the focus is on determining what types of assets can be distinguished with multi-spectral imagery and could feasibly be recognised with a high degree of accuracy through an automated machine learning process. A summary of this pilot study is reported in Appendix B.

The industries reviewed include: agriculture, heavy industry, mining, oil and gas extraction, the power sector, and retail and commercial industries. The industries assessed in this pilot collectively comprise a majority of the world's GHG emissions, accounting for approximately 65% of global emissions. The power sector, heavy industry, mining, oil and gas extraction make up around 55% of the world's CO_2 emissions. Furthermore, the agricultural industry is the biggest anthropogenic contributor of NO_2 and methane accounting for approximately 75% and 40% of global emissions respectively.

In this pilot study asset features that are visible on aerial imagery (Google Earth) and satellite images (Sentinel 1, 2 and Landsat 8) are established. This was achieved by identifying the different types of sites that fall under a sector, outlining their differences in production technologies and looking for recurring features. A focus was placed on identifying features relevant to the scope of the project, meaning the identification should add to our understanding of those sites, and ideally give an indication of the technology in use, to facilitate the identification of changes in greenhouse gas (GHG) emissions and any environmental impacts. After identifying the most promising ideas, three general concepts were tested, namely: activity monitoring, area/extent monitoring and asset identification.

5.1. Agriculture

Types of Products:

- Arable farmland (huge areas without any buildings or other detectable features).
- Cattle farms, chicken farms, pig farms (areas with large buildings).

Features:

- Recurring features:
  - Large buildings, most of the times in a specific systematic pattern.
  - Sometimes wastewater treatment and collection basins.
- Visible features in Sentinel 2:
  - Buildings are visible, but not very well due to the limited spatial resolution.
  - Wastewater treatment basins are not visible in Sentinel 2 imagery.

Summary:

- Livestock farms are difficult to identify from aerial or satellite images as many are outdoor and spread over very large areas (e.g. ranches), while some are indoors (e.g. farms). In both cases, the extraction of information is challenging due to large differences in their appearance.
- However, as outlined in the previous section, it is possible to use the ESA CCI classification map to identify croplands (see Section 4.1). Using the ESA's CCI land cover map a distribution of the local, regional and global croplands can be obtained. Temporal changes to the size and utilisation of croplands can be tracked over time as the ESA CCI map is updated.

Figure 6: Imagery of Two Farms

Two farms as seen from aerial imagery. As explained above, satellite imagery of such sites does not allow the identification of recurring features, which reveal information specific about the company or site.

5.2. Heavy Industry

5.2.1. Aluminium Electrolysis & Exclusion

Aluminium production with integrated alumina production & red mud disposal:

- Recurring features:
  - Characteristic red mud disposal sites, covering large areas.
  - Very long and rectangular buildings (similar to glass manufacturing buildings).
  - Almost always at the seaside.
  - Close by power plant (coal [with stockpiles], hydro, oil, gas, etc.) or very distinct infrastructure for power retrieval (power lines, masts, transformer stations).
- *Visible features in Sentinel2*:
  - Elongated production buildings.
  - Red mud disposal sites are clearly visible in TrueColor, SWIR and NIR.

Figure 7: Imagery of an Integrated Alumina Production Site
Mine with red mud disposal shown with a true colour image (top left), with SWIR (top right) and with NIR (bottom). Using either of these composites the red mud can be tracked and classified (e.g. green colour in bottom image).

5.2.2. Cement

Types of plants:

- With quarrying on-site (dry → wet)
- Transport of limestone to the site (dry → wet)

On-site mining:

- Recurring features:
  - Most sites are connected by train or ship.
  - Each site has stockpiles of coal, sometimes below a roof.
  - Occasionally (mainly in the US) cupolas are used to store clinker.

Only cement manufacturing:

- Recurring features:
  - Same as for on-site mining, but without quarries or with closed quarries.
  - Google Earth imagery can be used to decide whether a quarry is active or not (machinery movements, vegetation on slopes etc.).
- Visible features in Sentinel 2:
  - Multi-temporal imagery could be used to detect temporal variations, indicating potential quarry activity.

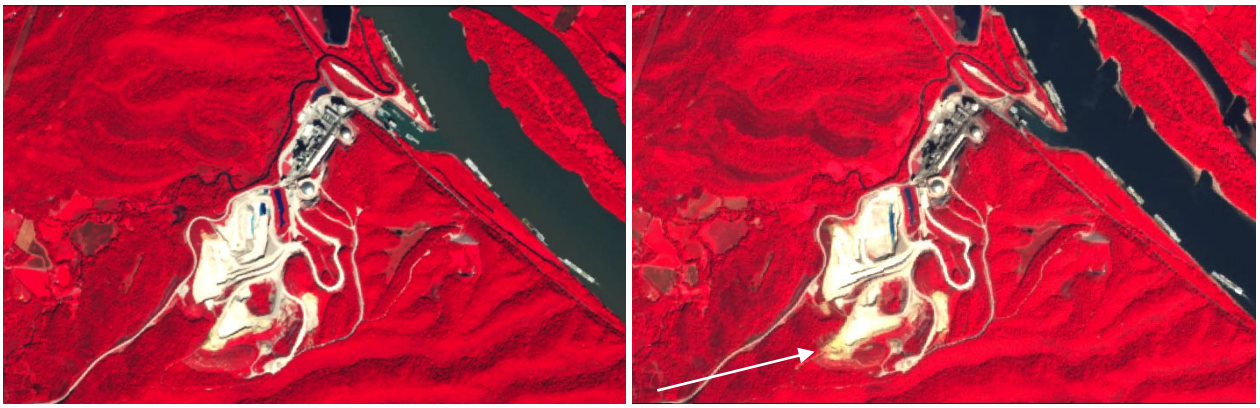

Figure 8: Imagery of a Cement Plant and Limestone Mine
Cement plant and limestone mine in 2016 (left) and 2017 (right). The growth of the mine can be seen in the pictures but this provides limited information about the technology used on site. High resolution imagery may be helpful for the identification of excavation methods, but not whether the cement plant is using dry or wet processes.

Summary:

- Emissions in the cement sector mainly depend on the type of process used (wet or dry), the pyro-processing and the transport of limestone to the site. The first two are not identifiable using aerial imagery of Sentinel data. Some sites have mining and quarrying on site, while others (often those located closer to cities) don't. The presence or absence of mining on site can be identified through aerial photography (moving machinery or vegetation on quarry walls) and possibly using satellite data (using temporal imagery to detect increase in mine extent).
- Coal stockpiles can also be identified, although some plants have these stockpiles under roofs.
- Cement plants that are found in large industrial areas or cities are more difficult to explore using satellite data.
- Potentially, the locations could be "tested" using satellite imagery to check if the location is a cement plant, instead of an office building. This could be done by classifying by shape and colour (based on the idea that houses are identified as smaller shapes). However, this would be difficult/time consuming, however.
- Better spatial resolution would not significantly increase the ability to identify sites.

5.2.3. Chemicals & Industrial Processes

Chemicals Sector: Establishments classified in this major group manufacture three general classes of products: (1) basic chemicals, such as acids, alkalis, salts, and organic chemicals; (2) chemical products, chemicals to be used in further manufacture, such as synthetic fibers, plastics materials, dry colours, and pigments; and (3) chemical products to be used for ultimate consumption, such as drugs, cosmetics, and soaps; or to be used as materials or supplies in other industries, such as paints, fertilizers, and explosives.

Chemical plants:

- Recurring features (only for very large plants):
  - Storage tanks (possibly for oil)
  - Coal stockpiles (e.g. at Sadara and Antwerp)
  - Water bodies (possibly for wastewater treatment)
  - Power plants on site (coal, etc.)
- Visible features on Sentinel 2:
  - Some flares (on very big plants)

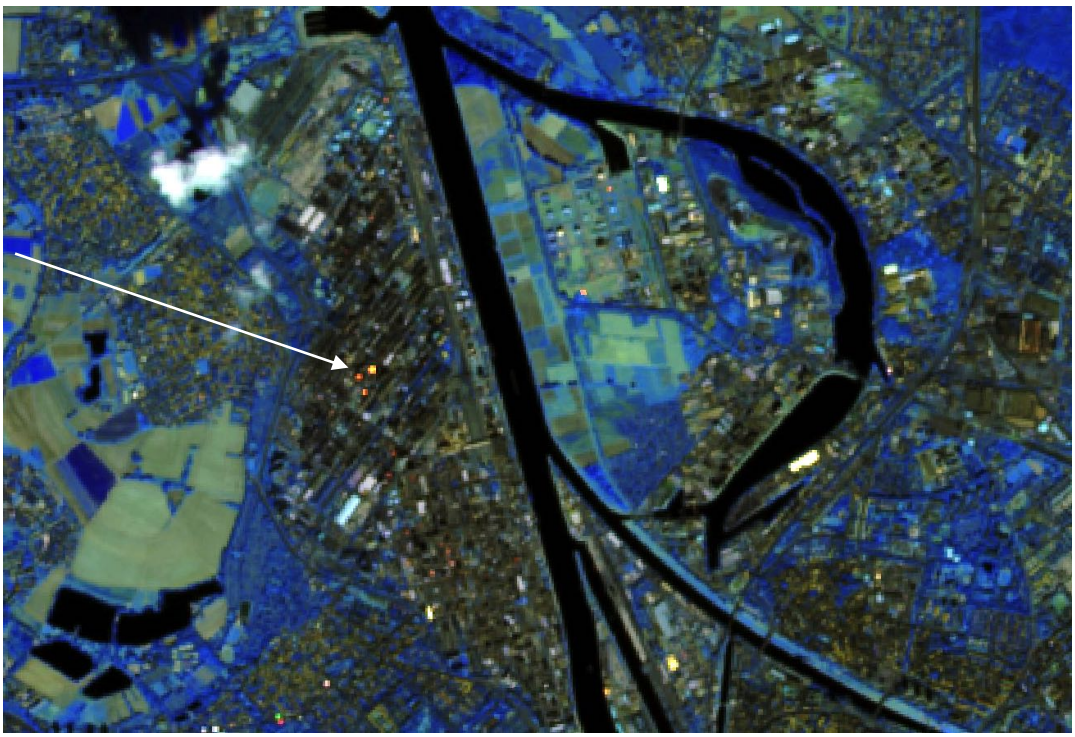

Figure 9: Imagery of a Chemical Plant
On very large chemical plant sites, flares can be identified by using NIR or SWIR bands (indicated by arrow).

Summary:

- As the sector "Chemicals" is extremely broad, there are no recurring features that could be identified from satellite images. A large percentage of chemical plants appear simply as buildings, often in industrial areas without any specific indication of what chemical product is being produced and what technologies they may be using. However, some very large chemical plants (e.g. Sadara in Saudi Arabia) have their own power plants and water treatment on site. For these types of plants, coal stockpiles and flares can be detected using Sentinel 2 to approximate the power sources and amounts of fuels used but no indication on the type of technology and/or chemical products can be obtained.
- Imagery with a better spatial resolution would not facilitate the identification of features, as the main limitation is the complexity of the sites and assets.

5.2.4. Oil Refining & Upgrading

Types of Products:

- LPG
- Petroleum Naftha
- Gasoline
- Diesel
- Heating oil

Oil Refinery sites:

- Recurring features:
  - Close to power stations
  - Towers/Chimneys (possibly cooling towers)
  - Oil storage tanks (circular)
  - Often very close to water, or on the sea shore (due to large water requirements)
- *Visible features in Sentinel 2:*
  - Oil Tanks (counting and possibly surface area measurement)

Summary:

- The only detectable characteristic of petroleum refinery plants is the presence of circular storage tanks as well as the proximity to the sea and power plants. Using all three criteria, petroleum refinery sites could theoretically be detected and located automatically. The identification of products at each site requires high resolution imagery to detect specific equipment. However, the complexity of this may not allow for its automation.

5.2.5. Pulp & Paper

Types of factories:

- **Integrated mills** = produce own pulp (pulping + bleaching) and use it for paper production (on the same site, receive logs or wood chips, usually stockpiled without roof).
- **Non-integrated mills** = get pulp from another site (receive pulp, usually stockpiled below a roof, but not necessarily).
- Pulping can be done
  - **with chemicals**
  - **mechanical**
- Prior to paper manufacture pulp is **bleached.**

Integrated mills:

- Recurring features:
  - Large stockpiles (logs, wood chips, pulp, etc.) on site and occasionally stockpiles of coal for on-site energy production.
  - Integrated mills are always close to water bodies because they need lots of water
  - Locally associated with large tanks for bleaching etc.
  - Always associated with wastewater treatment basins.
- *Visible features in Sentinel2*:
  - Wood chips are visible in NIR and SWIR, logs are visible in the red edge IR (8,8A).
  - Energy production on site is not visible with Sentinel 2 NIR bands (possibly a result of the chimneys being too small).
  - Locally stockpiles of coal are visible with NDWI, NIR and moisture.
  - Wastewater basins are hard to identify with Sentinel 2.

Figure 10: Imagery of a Pulp Factory
Pulp factory in red edge using Sentinel 2, arrow indicates a wood stockpile in brown.

Non-integrated mills:

- Recurring features:
  - No recurring features identified other than buildings
- *Visible features in Sentinel2*:
  - None

5.2.6. Glass

Types of sites*:

- Floating glass production sites (for construction, cars, etc., producing sheets of glass).
- Glass blowing production sites (for food industry etc., producing bottles, jars).

*The two types of production sites cannot be distinguished from each other in air- or space borne imagery and are treated as one category. Both use raw materials (such as sand, dolomite, fly ash, etc.).

Glass production sites:

- Recurring features:
  - Open-air stockpiles of raw materials are not common, raw materials are stored in vertical tanks with small diameter but large height.
  - Factory buildings are always rectangular and elongated, probably due to the requirements of the floating glass production machinery (one long conveyor belt/floating basins).
  - Manufacturing processes all take place under roof.
  - Production sites have a high energy demand and are always either situated very close to power plants, produce their own energy (chimneys are visible at those sites) or have distinct power infrastructure (transformers etc.).
  - A common characteristic feature is not present (other than the building shape, which could be confused with aluminium production).
- *Visible features in Sentinel2*:
  - Chimney activity cannot be identified.
  - Stockpiles (if present) cannot be identified, because they are too small.
  - Elongated buildings are clearly visible, but could be difficult to track, as some factories have factories have homogeneous roofs that could confuse automated detection.

Summary:

- Both different glass production factory types cannot be distinguished using air- or spaceborne imagery.
- Factories appear to stockpile raw material inside or in vertically elongated containers/tanks, which impedes detection.
- All glass factories have rectangular and elongated buildings that can be recognised in Sentinel 2 images. However, roofs are homogeneous and could therefore confuse automated detection codes. Further, the elongated factories could be confused with aluminium factories.
- Glass factories have a high energy demand and are always either situated very close to power plants, produce their own energy (chimneys are visible at those sites) or have distinct power infrastructure (transformers etc.). Chimney activity cannot be seen in Sentinel 2 imagery. Some sites appear to use solar power as well, so multi-temporal high-resolution imagery could be used to monitor the distribution of these panels on the roofs of glass factories.
- All in all, detection with Sentinel 2 would be only possible based on the building shape, but the reliability of this method is unclear due to similarities with other sectors.

5.2.7. Iron & Steel

Summary:

- All production steps are performed inside or below a roof, but stockpiles can be identified in high-resolution imagery. However, stockpiles, if present, are relatively small and cannot be identified with Sentinel 2 images. Therefore, investigations related to stockpile composition or extent have to be performed with high-resolution imagery.
- Sentinel 2 NIR bands could potentially be used to detect factory activity (e.g. by sub-setting the chimneys and scanning for highly reflective NIR band pixels).
- A time series analysis of two subsets of Tata Steel NL and Nucor Steel US suggests that Sentinel 2 can be used with NIR bands to monitor factory activity (activity of on-site energy production e.g. by burning coal + activity of kilns, ovens etc.) (on/off) with the main limitation being cloud cover. Using high-resolution imagery, the sources of the IR emission can be identified. Subsequently, IR emissions could be correlated to activity of certain parts of the factory (such as energy production, kiln activity etc.) potentially giving hints about the production.

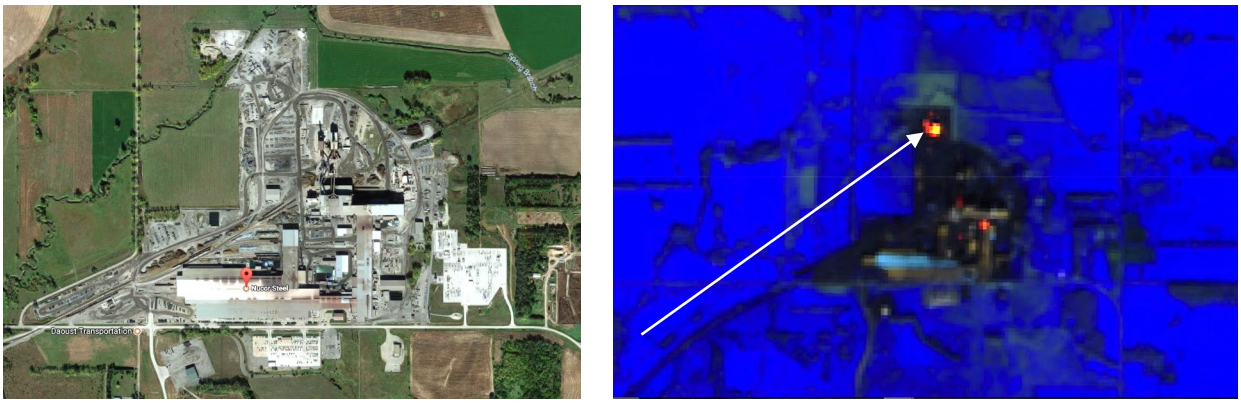

Figure 11: Imagery of a Steel Factory
True image (left) and Sentinel bands 12,4,2 (right) of a steel factory. The only detectable feature is the flame (red spots on right picture), which may be used to track the activity (on/off) of the factory.

5.3. Mining

5.3.1. Bauxite

Bauxite mines:

- Recurring features:
  - Very characteristic red colour of bauxite (true colour).
  - Machinery can be seen in high-resolution imagery (excavators, trucks etc.).
- *Visible features in Sentinel2*:
  - Can easily be distinguished from the surroundings with true colour (red), SWIR (violet or pink), and NIR (beige) bands.
  - Bauxite mine extraction can be monitored over time, because most mines are shallow and grow horizontally rather than vertically.

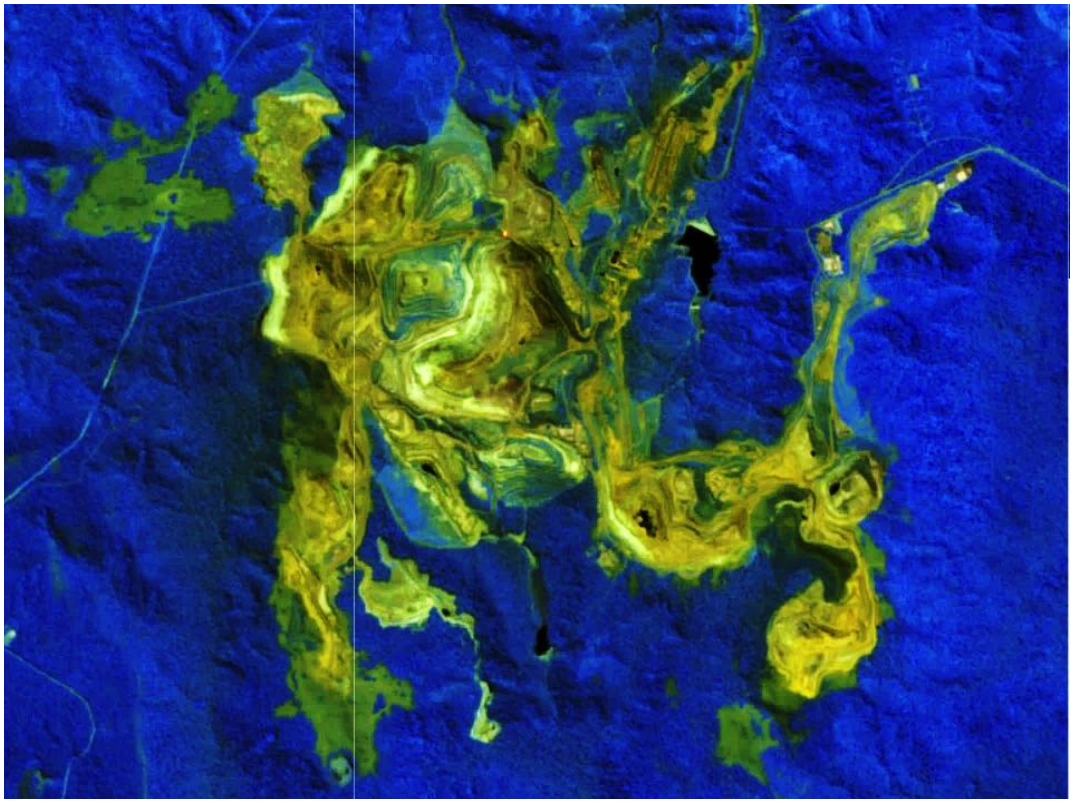

Figure 12: Imagery of a Bauxite Mine
Bauxite mine seen with NIR bands on Sentinel 2 imagery. The image shows that due to the characteristic colour and reflectance of the dug-out ground, one can see the extent of the mine (brownish).

5.3.2. Coal

Types of mines:

- Underground
- Surface mining (huge machines)
  - Rotary excavators/Dragline
  - Mountaintop removal
  - Open-Pit

Underground coal mines:

- Recurring features:
  - Stockpiles of coal (black colour)
  - Circular basin (possibly for cleaning or grinding)
  - Pipes/conveyor belts
  - Water bodies (small lakes)
- *Visible features on Sentinel2*:
  - Black stockpiles (using band combinations 02 11 8A + Moisture [(B8A-B11)-(B8A+B11)] + NDWI [(B3-B8)/(B3+B8)]). Computing the size of the stockpile, it is possible to see changes in productivity.
  - Stockpiles are not always present; other storage technologies are not visible on Sentinel.
  - Features like basins and conveyor belts are too small to be visible on Sentinel.

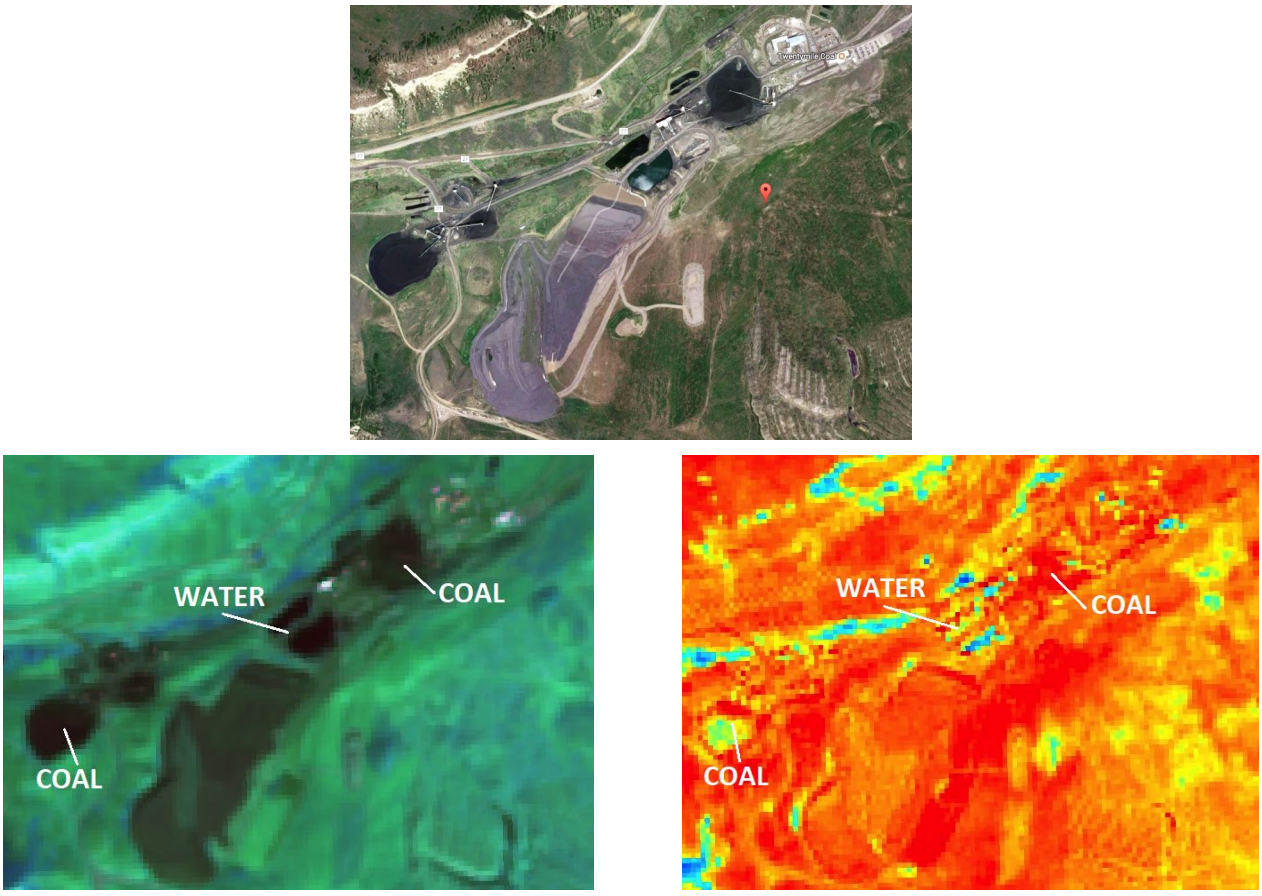

Figure 13: Imagery of an Underground Coal Mine
Three images of the same underground coal mine (top: true colour image, bottom left: NIR, bottom right: moisture) indicating the process by which one can identify coal stockpiles. The NIR filter shows both water and coal stockpiles in the same colour, while the moisture filter identifies only water bodies. Subtracting the moisture filter from NIR, an algorithm can be used to detect coal stockpiles, measure the surface area they cover and understand how the mine's activity may be changing over time.

Surface coal mines (dragline):

- Recurring features:
  - Affected area (Light-coloured soil lines)
  - Stretched out stockpiles
  - Water body (variable size depending on the site)
- *Visible features on Sentinel2*:
  - Stockpiles (as described above for underground mines and using NDWI to locate coal piles and them moisture index to remove water bodies)
  - Affected area (using vegetation index (B8 - B4)/(B8 + B4))

Figure 14: Imagery of a Surface Coal Mine
True colour image (left) and NDWI composite (right) of a surface coal mine. Detection of a surface coal mine can be done with a vegetation filter as well, especially in cases where mines are in vegetated areas and therefore create a big contrast with their surroundings.

Summary:

- Mines are often in areas that have small cities nearby, therefore any image processing would have to contain careful separation of what falls under the classification of a "mine".
- Sentinel 2 can be used to detect coal stockpiles, if present, using certain band combinations. A better spatial resolution would not provide more information for stockpile identification. Some mines do not stockpile or stockpile below roofs. The presence of clouds significantly impedes stockpile identification.
- The difference in the shape of the stockpile can be used as an indication of the type of mine (surface (long, narrow) vs underground (circular)).
- Note that in surface mines, what we identify as "stockpile" may not always be stocked coal, but may be in-situ coal of recent excavations.
- High-resolution imagery (Google Earth) is useful to recognise machinery/technology (such as excavators, draglines, rotary excavators etc.).
- Generally, clouds are an obstacle for any frequent observation/detection of features/changes.
- Due to the large spatial extent of surface extraction sites, frequent classification in combination with subtraction could give a constant estimation of productivity, dependent on cloud coverage (using Sentinel 2) (using 04 04 04 red edge with high gamma and low gain as a semi-binary interpreter).

5.3.3. Gold

Gold Sites:

- Recurring features:
  - Grounding and rinsing basins on-site to separate gold from the host rock.
  - Large disposal sites for remaining host rock (tailings), gold content in host rock is normally below 1% → large amounts of tailings are produced.
- *Visible features in Sentinel 2*:
  - Rinsing basins are visible in Sentinel 2 data, but not particularly well, due to their size.
  - Rinsing pools and tailings do not have a characteristic spectral response, which impedes reliable detection.

5.3.4. Uranium

Uranium Sites:

- Recurring features:
  - Rinsing basins are present in the mines to separate the host rock (tailings) from the uranium.
  - Large disposal sites for remaining host rock (tailings), uranium content in host rock is very low → large amounts of tailings are produced.
- *Visible features in Sentinel 2*:
  - Rinsing basins are visible in Sentinel 2 data, but not particularly well, due to their size.
  - Rinsing pools and tailings do not have a characteristic spectral response, which impedes reliable detection.

5.3.5. Iron Ore

Iron Ore Sites:

- Recurring features:
  - Reddish colour of the iron-rich soil
  - Pools (cleaning and waste disposal)
- *Visible features in Sentinel 2*:
  - By using bands R:04,G:04,B:04, we can classify (in semi-binary mode) the mine. Then, by defining a subset/polygon around the possible extent of the mine, temporal images can be used to track the extent of growth.

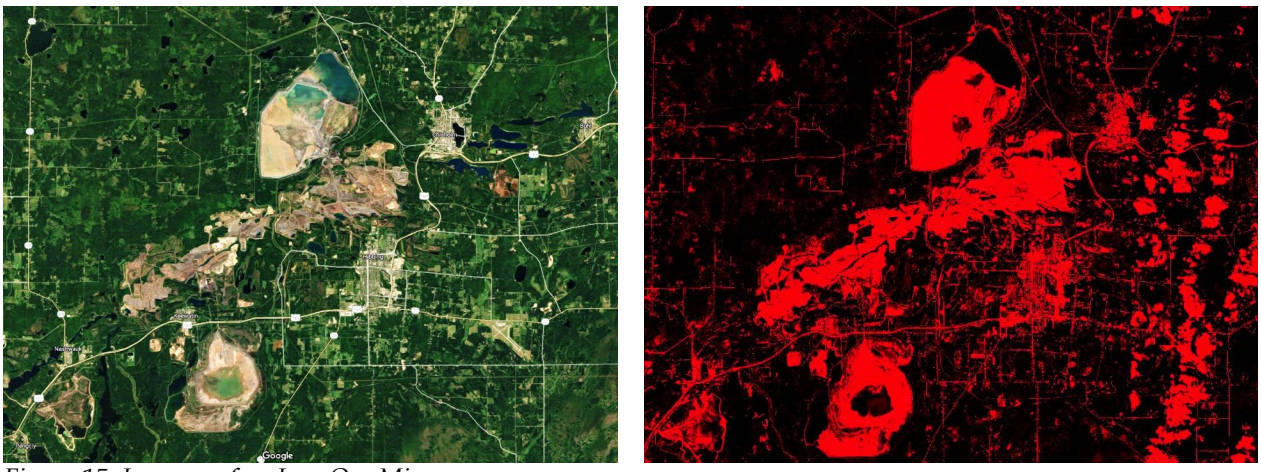

Figure 15: Imagery of an Iron Ore Mine
A semi-binary classification indicates the extent of an iron ore mine and can be done temporally to track growth/activity.

5.3.6. Diamond

- Recurring features:
  - Cyclonic separation basins that separate the ore from the diamonds using gravity
- *Visible features in Sentinel 2*:
  - Cyclonic separation basins are visible in Sentinel 2 images, but with certain limitations, caused by the poor spatial resolution

Figure 16: Imagery of a Diamond Mine
True colour image (left) and IR image (right) of a diamond mine. Detection of the extent of diamond mines is possible using IR bands, but the expansion is usually very slow (since they are mainly underground) and may not provide much information relevant to the project's scope.

Summary:

- Gold mining uses mercury and nitric acid to separate and process the final product, both of which can have large environmental impacts. The disposal site of these is clearly visible, usually at a proximity to the gold mine, with the presence of some pools. The automatic detection and calculation of the surface covered by these disposal sites may be difficult as they often have similar spectral responses to the mine itself. The detection of rinsing pools is possible using Sentinel 2, but limited by their relatively small size. As they don't have a characteristic spectral response either, their detection is impeded as well.
- Multi-temporal image stacks could be exploited to analyse gold, uranium and diamond mine evolution over time, but as these mines go usually deeper instead of wider, results are not expected to be particularly good (using 04 04 04 red edge with high gamma and low gain as a semi-binary interpreter).
- Uranium mining uses acids and bases to separate and process the final product, both of which can have large environmental impacts. The disposal site of these is clearly visible, usually at a proximity to the uranium mine, with the presence of some pools. The automatic detection and calculation of the surface covered by these disposal sites may be difficult as they often have similar spectral responses to the mine itself. The detection of rinsing pools is possible using Sentinel 2, but limited by their relatively small size and number. As they don't have a characteristic spectral response either, their detection is impeded as well.
- Diamond mining uses ferrosilicon & water solution and cyclones basins to separate and process the final product. The disposal site of the by-products is clearly visible, usually at a proximity to the diamond mine, with the presence of some pools. The automatic detection and calculation of the surface covered by these disposal sites may be difficult as they often have similar spectral responses to the mine itself. The detection of cyclone pools is possible using Sentinel 2, but limited by their relatively small size and number. As they don't have a characteristic spectral response either, their detection is impeded as well.

5.4. Oil & Gas Extraction

Methods:

- Off-shore
  - Drillship
  - Semi-submersible
  - Jack-Up Rig
  - Drilling Barge
- On-shore (classic drilling rig)
  - Landrig (liquid oil)
  - Shale oil
  - Tar sands / Oil sands (different methods)

Ideas:

- Look at a platform that is on secondary recovery stage and look at before and after images, to identify methods by which we can detect the stage of oil recovery of each site (on-/offshore).

Off-shore sites:

- Issues with off-shore rigs:
  - Non-constant locations
  - Scarce information on coordinates
  - Difficult to attribute each location to specific companies
  - Using radar, we can locate off-shore locations around oil-reserves (through clouds) but cannot see any features signifying change (frequent location extraction but no information about type, company, activity, etc.)
  - Using Sentinel 2 with NDWI and NIR bands oil platforms can be easily detected, only limited by cloud cover
  - NIR bands of S2 might indicate chimney activity (productivity estimation?)

On-shore oil production sites:

- Conventional oil extraction:
  - Recurring features:
    - Circular tanks (visible only on aerial photos, sometimes in Sentinel 2, if large enough)
    - Flaring of gas (CH4)
  - *Visible on Sentinel 2*:
    - Possibility to classify oil/shale gas field extent using soil brightness (indicating roads vs soil), could be an indication for a growing extraction & production (potentially in combination with flare counting).
    - The presence (or absence) of flares (Sentinel bands 12,4,2) can indicate whether the site captures or re-injects natural gas.
    - Using sentinel bands NIR+8A, we can identify flares off-shore. Combining this with radar images we can identify where off-shore sites exist. (main limitation: clouds)
    - Pump jacks are not visible through sentinel

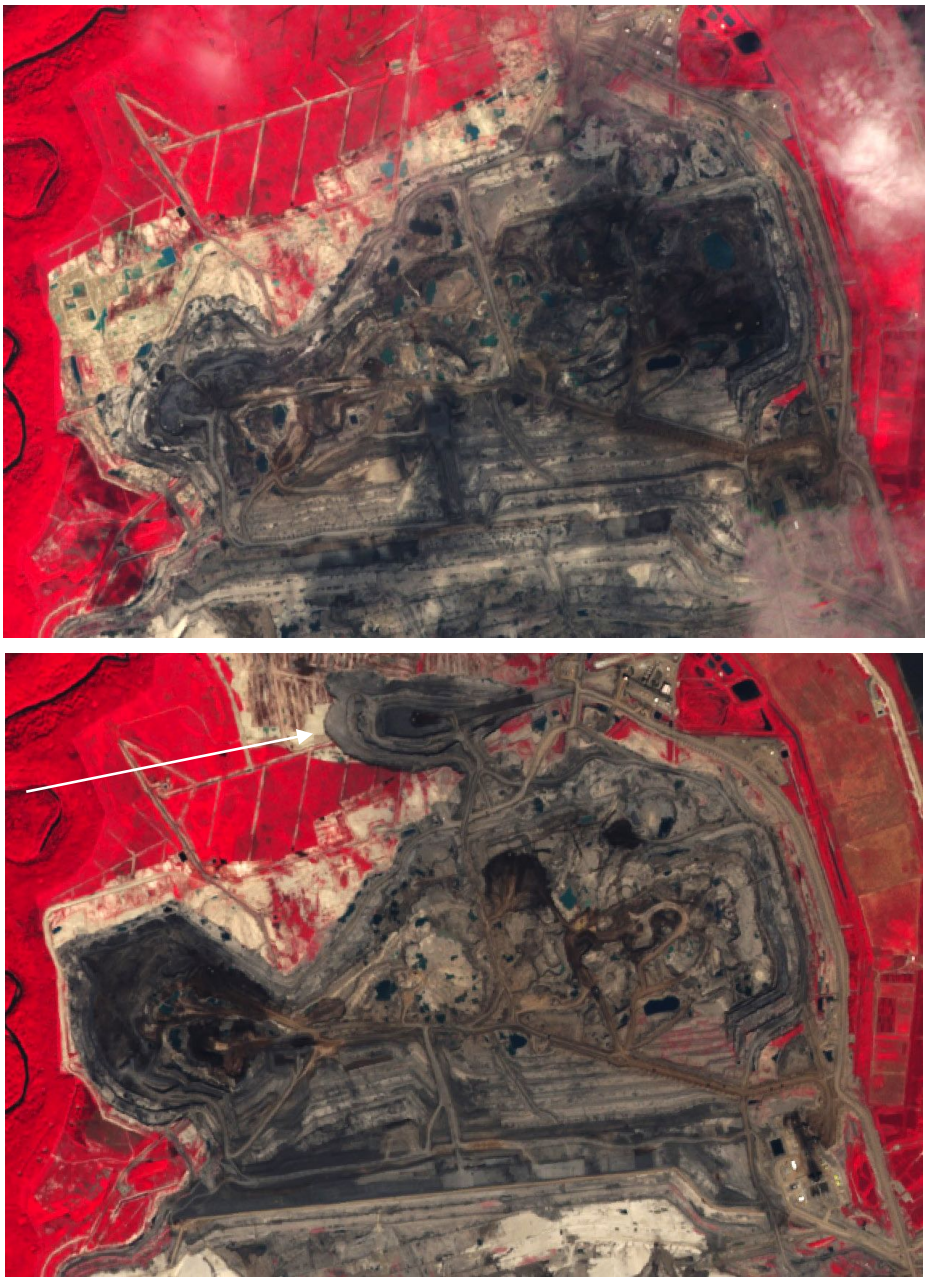

Figure 17: Imagery of the Athabasca Tar Sand Field
Athabasca tar sand field shown in 2016 (top) and 2017 (bottom). Infrared bands in sentinel allow for a classification and correct separation of the mine and the surrounding environment. A multi-temporal analysis (e.g. annual) can allow the tracking of surface area covered or the expansion of the mine.

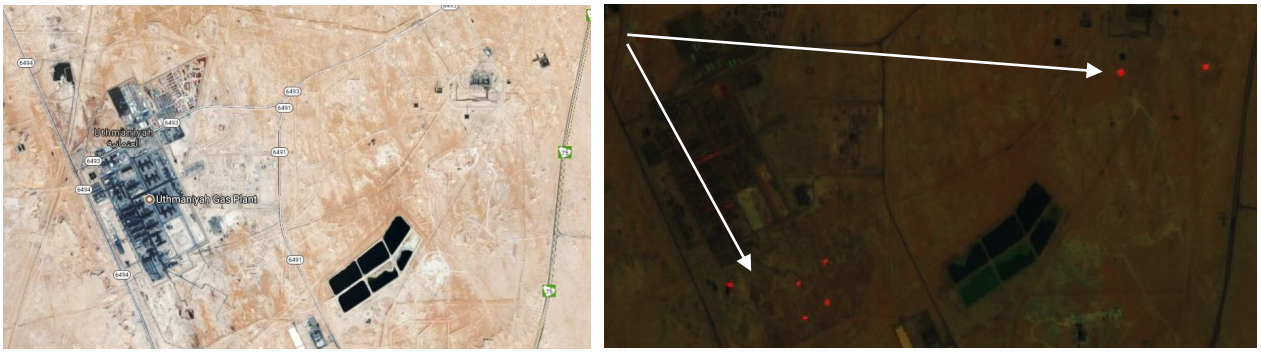

Figure 18: Imagery of an Oil Field
True colour image (left) and Sentinel bands 12,4,2 (right) of an oil field (Ghawar, Saudi Arabia). The bands 12,4,2 on Sentinel 2 indicate the position of flares on site, and can be indicate field activity (on/off) of the site.

Summary:

- **Offshore**: oil platforms are not contained in Google Earth imagery but are visible in Sentinel 2 with NDWI and NIR bands, however visibility is limited by intense cloud cover. Sentinel 1 radar can be used to locate all barges, platforms, etc. and track them over time, but cannot recognise type, owner, or any other details. By using multi-temporal images ships (moving) could be distinguished from platforms (not moving). In addition, Sentinel 2 (NIR+8A) can be used to detect flaring platforms to verify Sentinel 1 findings and to measure platform activity, but heavily dependent on cloud cover.
    - Time series analysis of a Norway subset suggests that Sentinel 2 can be used with NIR bands to monitor offshore oil platform activity (on/off) with around 2 images per month, limited by cloud cover. The results from Norway further indicate that platform location extraction with Sentinel 2 is significantly limited due to clouds and could be performed roughly once a year by mosaicking cloud free images.
- **Onshore**: oil fields in various locations appear to have round storage tanks as common features, but can only occasionally be detected with Sentinel 2 due to size limitations. However, gas flares can be recognised and could give a measure of field activity (counting) and extent (assume a circle around each flare with a derived mean distance, which covers the oil field). Classification and subtraction of light sand fields and roads in contrast to either the surrounding soil or darker soil within the oil field based on Sentinel 2 imagery could give a temporal measure of oil field activity (growth).
- **Shale gas field:** Gas flares can be recognised as well and could give a measure of field activity (counting) and extent (assume a circle around each flare with a derived mean distance, which covers the shale gas field). Classification and subtraction of light soil fields and roads in contrast to either the surrounding soil or darker soil within the shale gas field based on Sentinel 2 imagery could give a temporal measure of activity (growth). Extraction and injection locations could be distinguished by using high-resolution imagery (e.g. aerial imagery, looking for sites with tanks, pipes etc. and sites with only injection holes, which cannot be identified with Sentinel 2), giving an idea of relation between injection and extraction = shale gas field productivity and reserves.
- **Oil sands/ tar sands:** flares can be recognised as well and could give a measure of field activity (counting). Due to the large spatial extent of the extraction sites, frequent classification in combination with subtraction could give a constant estimation of productivity, dependent on cloud coverage (using Sentinel 2).

5.5. Power Sector

5.5.1. Coal

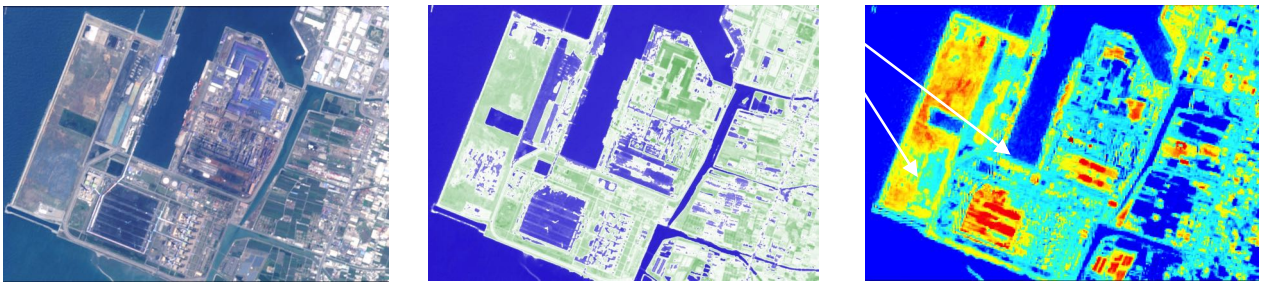

Figure 19: Imagery of a Coal-Fired Power Plant
True colour image (left), NDWI (middle) and moisture composites (right) of a coal-fired power plant. By comparing moisture with NDWI, we assume that an automatic algorithm could be set up to potentially identify and track coal stockpiles.

Similar to coal mines, stockpiles of coal can be identified and tracked temporally to detect size changes (not precisely due to a lack of spatial resolution), using the NDWI and Moisture index. A possible issue is that often power plants do not only burn coal, and therefore other black shapes may be detected. Additionally, we can see the number and size of chimneys at each coal-fired power plant, especially through aerial imagery. The presence of clouds and application of low resolution imagery makes this detection difficult using Sentinel 2 images. An automated detection could target the stockpiles of the power plants quite effectively using the same method as coal mines.

5.5.2. Gas

Identification of gas plants is generally difficult; due to a lack of stockpiles and as power plants appear to have thin chimneys that are not visible in Sentinel 2 images. Additionally, detection of gas tanks is difficult, as the resolution is not adequate. Indicators are power lines and potentially high chimneys (only their shadows might be visible with Sentinel 2). Using high-resolution imagery, identification is much easier, but automated detection does not appear to be possible based on currently available imagery.

5.5.3. Oil

Oil plants are characterised by huge oil storage tanks, which are clearly visible in Sentinel 2 imagery. Further indicators are power lines and potentially high chimneys (only their shadows might be visible with Sentinel 2). Using high-resolution imagery, identification is not any easier. An automated identification could be done using colour- and object based storage tank detection. Using pixel size and counting, one can approximate the oil storage capacity of each plant.

5.5.4. Nuclear

There are no common features between nuclear plants. Although the reactors can be identified through aerial imagery, they vary in shape and size between sites, making automated identification impossible. In addition, all locations of nuclear power plants are known and fuel type and shape do not change. However, high-resolution imagery could be used to check the progress of construction of new plants or expansions of existing plants (Sentinel 2 data is not useful for this application).

Figure 20: Imagery of a Nuclear Plant
High resolution imagery (aerial, Google Maps) of a nuclear plant. Features specific to such plants are difficult to distinguish from their surroundings.

5.5.5. Solar PV

As solar PV cells have a very particular appearance from space, we wanted to test whether an unsupervised classification of a region (with a solar park) can help the automatic identification of such panels. If successful, this process can be automated and done temporally to track changes and growth of solar parks.

Unsupervised classification (e.g. with k-means) also delivers very good results with very few mis-interpretations, using only RGB bands. The spatial resolution of Sentinel 2 is sufficient to resolve arrays of solar panels, although no single cells can be identified. Using this classification technique, over time the spatial extent can be measured and potentially correlated to power production.

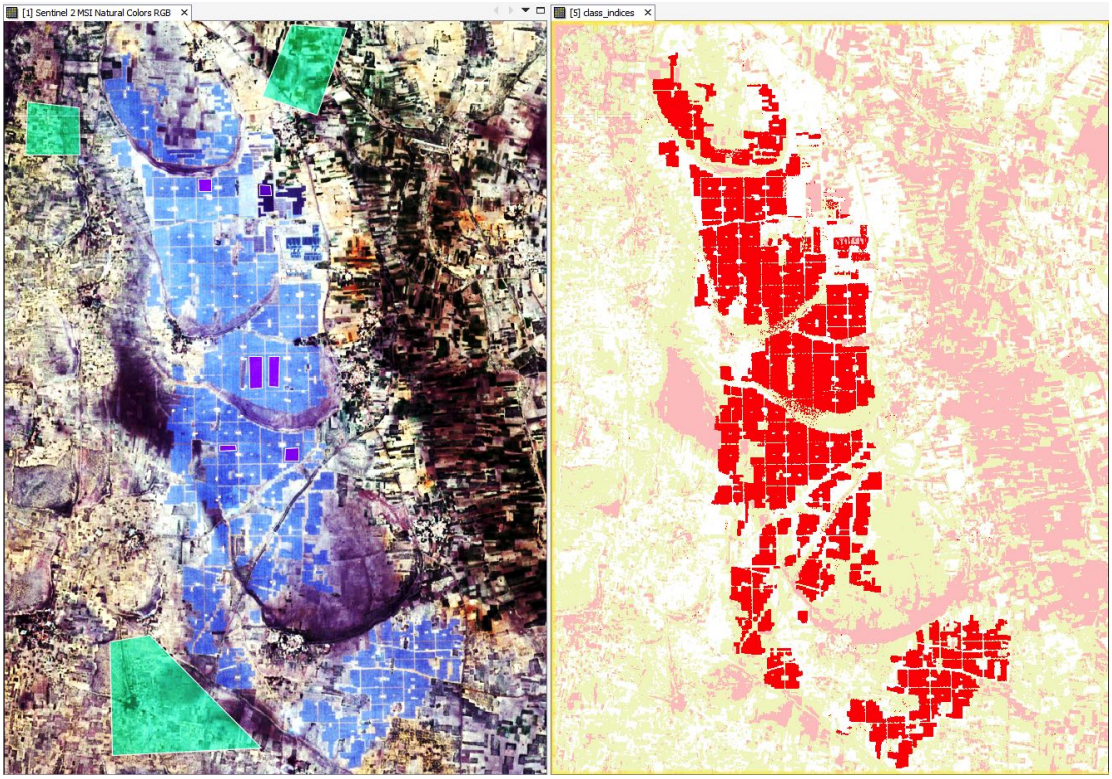

Figure 21: Imagery of Solar Panels (1)
Unsupervised classification of solar panels using Sentinel 2. Note: the code detects classes in an unsupervised manner, but the manual testing of the number of classes best depicting this can be considered some sort of supervision and could potentially change from site to site.

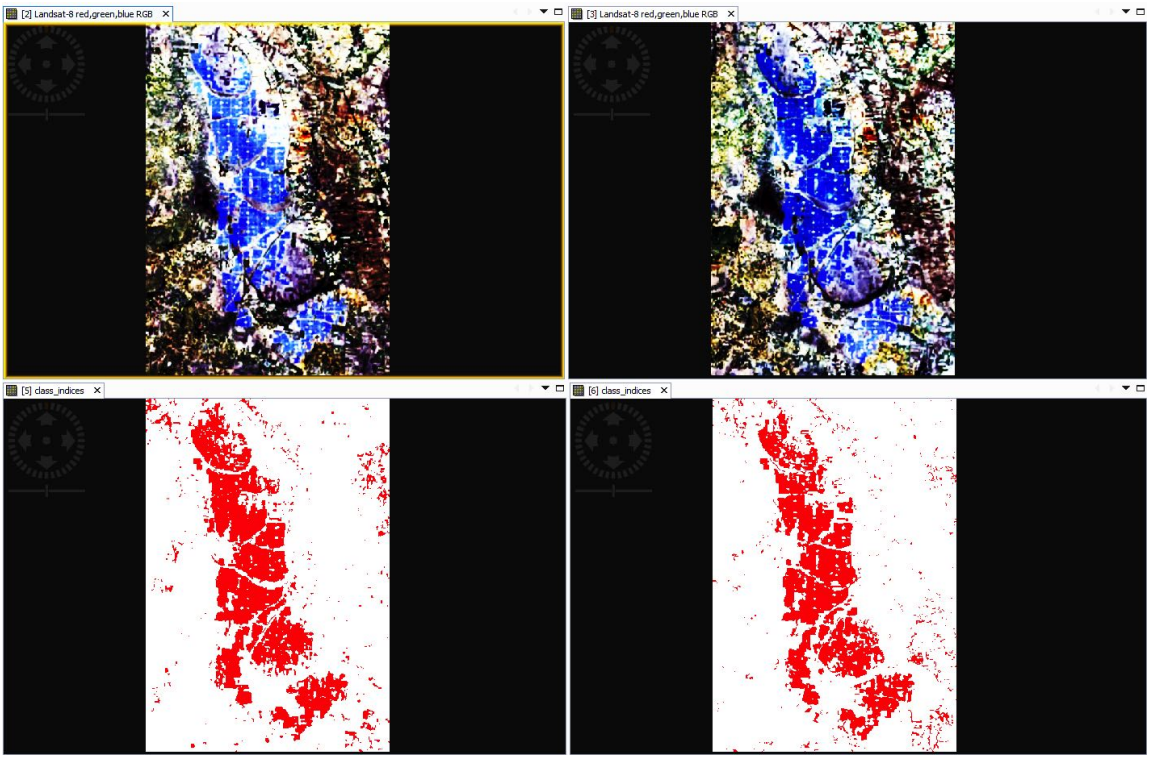

Figure 22: Aerial Imagery of Solar Panels (2)
The expansion of the solar park (shown as more red pixels) is identified by classifying the image into four classes with a subsequent binary masking of the class of interest vs. all other classes. Such analysis can be done on a temporal basis (e.g. bi-annually) to understand how and if PV cell arrays are increasing. The image above shows an unsupervised Landsat classification from 2016 (left) and 2017 (right).

5.5.6. Wind

Using GRD-level Sentinel 1 radar data, wind turbines are clearly visible. Using this imagery it is also possible to obtain information on the number of turbines present at a site and keep track of farm growth over time. Due to the limited spatial resolution, turbines can't easily be distinguished from ships or other floating metallic objects immediately, but as turbines are built in a regular pattern, radar signatures in between the grid of turbines are likely other objects (such as ships). Locally, the blades of the turbines are measured by the radar and could support identification. Using a satellite image processing like SNAP, precise coordinates of single wind turbines can be derived.

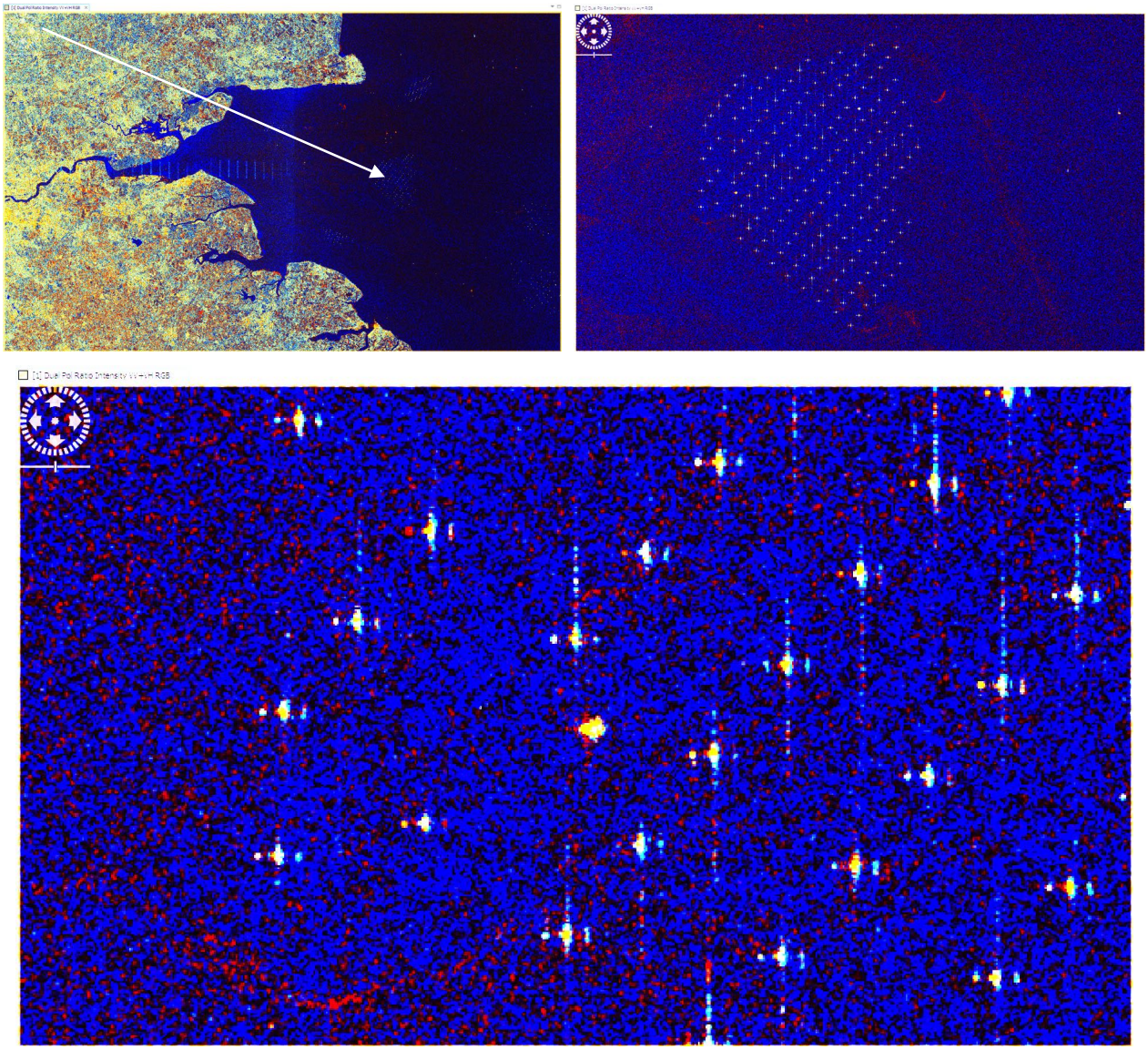

Figure 23: Imagery of a Wind Turbine Field
Sentinel 1 SAR image showing the coastline of London, UK. Location of the wind turbine field is marked with an arrow. The images above show the same area at different scales. The top picture demonstrates that wind turbines can be counted and their pattern identified, while the bottom picture shows higher details. In the last image, one can see what appear to be ships around the wind turbines.

5.6. Retail & Commercial

Recurring features:

- Parking lots (can be tracked with high resolution satellite imagery or aerial imagery but not with Sentinel 1 or 2).
- Other than parking lots, retail companies in satellite imagery mostly appear as buildings, and do not have many features that can be linked to change, or emissions.

Figure 24: Imagery of a Retail Location
Aerial imagery (left) and Sentinel 2 true colours (right) of a retail location, indicating the need for high resolution imagery in order to accurately make estimates about location activity and operations.

5.7. Overview

This pilot study establishes the feasibility of identifying and monitoring the activity of various industries. Most notably this study indicates that it is possible to monitor the activity of steel plants and oil fields, measure changes in the area covered by mines, tar sand fields, coal stockpiles and solar panels as well as to identify and locate off-shore wind farms and track their growth across time.

Based on this study the most promising sectors that are likely to be able to be identified through an automated machine learning process are mining, coal-fired power plants and croplands. Mines and the stockpiles can easily be distinguished from their surroundings using Sentinel 2 imagery. Furthermore, it is possible to identify the type of mine based on differences in the shape of the stockpiles (surface (long, narrow) vs underground (circular)) as well as the machinery/technology that is being used. Similarly, coal-fired power plants can easily be identified based on coal stockpiles as well as the number and size of chimneys. The stockpiles for both of these sectors can also be effectively monitored over time, which will facilitate the indirect measurement of GHGs. Finally, croplands can also be identified through the use of the ESA CCI classification map. The sizes and utilisation rates of these croplands can also be tracked over time as the ESA maps are updated. As a result of the ease of identification and the ability to perform temporal analyses these three sectors will be the primary focus for the next phase of the project.

6. Conclusion

Accurate asset-level data can dramatically enhance the ability of investors, regulators, governments, and civil society to measure and manage different forms of environmental risk, opportunity, and impact. Asset-level data is information about physical and non-physical assets tied to company ownership information.

We have focused on the potential role of remote sensing (and related technological developments such as machine learning) to secure better asset-level data and at higher refresh rates. In particular we focussed on using remote sensing to identify the features and use of assets relevant to determining their GHG emissions.

We find that the process of identifying and tagging assets (e.g. power generating stations, mines, farms, industrial sites) and asset-level features (e.g. cooling technologies, air pollution control technologies) can be automated through the use of machine learning. It is possible to train learning algorithms to recognise an asset and its features in remote imagery and then scan global imagery corpuses to identify all assets of that type. Human error rates are sufficiently low on these classification tasks that it is reasonable to expect these problems to be entirely automatable. With the exponential increase in space-based sensing, computing power, and algorithmic complexity, end-to-end learning systems are becoming increasingly available to academic researchers and the private sector alike. We expect that the development of a global catalogue of every physical asset in the world to be already within the reach of technical feasibility.

There are also viable methods using remote sensing data that could be implemented to measure asset-level GHG emissions too. These methods are: (1) a direct method, which involves the use of various sensors on spaceborne and airborne instruments to measure emissions directly; and (2) an indirect method, which utilises various identifiable asset characteristics to model GHG emissions.

The direct method of monitoring emissions requires the use of satellite or airborne instruments. Accurately monitoring GHGs from space is challenging because of their relatively small signal in comparison to other atmospheric constituents, but advances in both sensor technology and retrieval models are leading to more precise detection.

Direct emission monitoring is currently feasible for a relatively limited scope of assets (such as assets that are situated in regions with very few other sources of emissions in the surrounding area). However, the launch of the CarbonSat satellite in 2020 as well as some already scheduled sun-synchronous sensors offer the potential for more precise observation of GHG concentrations and emissions at the asset-level.

A complementary approach to direct measurement is to model GHG emissions indirectly using identifiable asset characteristics. This first requires the identification of key characteristics that are associated with GHG emissions. For example, asset utilisation rates are inherently linked to the level of GHG emissions. Using some of the spaceborne instruments in combination with real asset-level production data it is possible to model temporal variations in an asset's utilisation rate. Employing this projection of the utilisation rate an estimate of the emissions can then be obtained using a standardised model, such as those outlined in the IPCC guidelines.

The most notable drawbacks of the direct methods are the relatively low resolution of current instruments and the imprecise nature of the retrieval methods. The indirect method avoids these limitations associated with the direct method. The main drawbacks of the indirect approach are the ability to effectively identify asset characteristics and the accuracy of the modelling of the GHG emissions. Despite these potential impediments the indirect approach represents a more feasible method of measuring emissions based on currently available technology.

Through future research projects undertaken over multiple phases we plan to make asset-level data (including various technical features) and GHG emissions monitoring for each asset (using both direct and indirect methods) available for every physical asset in every sector globally, beginning with the most GHG intensive assets. We hope to create platforms for various users to access and use this data. This endeavour has the potential to transform how different actors in different parts of society measure and manage environmental risks, impacts and opportunities. It is enabled by significant public (and private) investment in data capture and remote sensing, which can now be brought together and processed in novel ways for direct application.

Glossary

Bayesian Error: The lowest possible prediction error that can be achieved for the classification of a random outcome and is the same as irreducible error.

Convolutional Neural Network: A type of neural network that has been used in the analysis of visual imagery.

Data Resampling: A statistical technique which involves the use of random subsets of available data with replacement for the estimation or validation of a statistical model.

Data Synthesis: A statistical technique that pools data from many different studies in order to obtain a more model than can be obtained from a single study.

Detection Machine: A machine that uses machine learning processes to classify or identify data into various categories.

Light Detection and Ranging (LIDAR): A surveying method that measures distance to a target by illuminating the target with pulsed laser light and measuring the reflected pulses with a sensor.

Machine Learning: A field of computer science that uses statistical techniques to give computer systems the ability to "learn" by using data, without being explicitly programmed.

Mosaicking: The process of unifying multiple images collected at different times or from different sources, which facilitates the comparison and combination of various images.

Multi-Class Classifiers: The classification of instances into one of three or more classes, in order to facilitate the prediction of a new instance into one of the classes.

Multi-Spectral Imagery: An image that captures data over a range of wavelengths within the electromagnetic spectrum.

Neural Network: A machine learning process that uses a large number of highly interconnected processing elements working in unison to solve specific problems.

OpenStreetMaps: A free editable map of the world, created by volunteers using open source content.

Orthorectification: A process of removing any effects associated with the tilt the image was taken at and adjusting for any terrain effects to create an image with a constant scale that can easily be processed.

Random-Forests: Is a machine learning method that uses a number of decision trees to classify data into two or more categories.

Shortwave Infrared (SWIR): The shortwave infrared section of the electromagnetic spectrum is typically defined as light with wavelengths between 900 to 3000 nanometers (nm). SWIR is similar to visible light in that photons are reflected or absorbed by an object, providing the strong contrast needed for high resolution imaging.

Support Vector Machines: A model of supervised learning used in machine learning for the analysis and classification of data into two or more categories.

Thermal Infrared (TIR): The thermal infrared section of the electromagnetic spectrum can be classified as any wavelengths between 3,000 to 100,000 nanometers (nm). TIR is in essence the heat radiation that is emitted from the surface of the Earth.

Training Data: A set of data that is used to initially fit the parameters of the model. The model that is fitted with the training data can then be validated and tested with other datasets.

Transfer Learning: A technique in machine learning that involves using the knowledge obtained from solving one problem for a different but related problem.

Visible and Near-Infrared (VNIR): The visible and near-infrared section of the electromagnetic spectrum is typically classified as wavelengths between 400 to 1400 nanometers (nm). VNIR includes the full visible spectrum band as well as a portion of the infrared spectrum.

Appendix A: Spaceborne Instruments for Monitoring Atmospheric GHG Concentrations

Mission	Launch	Orbit[95]	T. Cov.[96]	Spatial Scale	PS Det.[97]	GSD[98]	Measure Technique	Fitting window [nm]	Data Products	DT[99]	RP[100]
GOSAT	2009	ss	3	regional/continental	no	10	passive SWIR	1650, 2060	XCO_2, XCH_4	7.1	1 - 2
GOSAT-2	2018	ss	6	regional/continental	no	10	passive SWIR	1650, 2060, 2300	XCO_2, XCH_4, XCO	4.0	0.4
TROPOMI	2017	ss	1	global	partly	7	passive SWIR	2300	XCH_4, XCO	4.2	< 1
Sentinel-5/UVNS	2021	ss	29	global	no	7.5	passive UV/VNIR/SWIR	290, 400, 1633, 2345	i. a. XO_3, XSO_2, XCO, XCH_4	n.o.[101]	n.o.
OCO-2	2014	ss	16	global	partly	1.29 x 2.25	passive SWIR	1610, 2060	XCO_2	n.o.	< 0.3
TanSat	2016	ss	16	national/global	no	1 x 2	passive SWIR	1610, 2060	XCO_2	n.o.	< 1
GHGSat	2016	ss	14	local	yes	0.05	passive SWIR	1650	XCH_4, XCO	0.24	1
Bluefield	2019 - 21	ss	1	global	yes	0.02	passive SWIR	2300	XCH_4	0.015	0.8
CarbonSat	2020	ss	5 - 10	global	yes	2	passive SWIR	1650	XCH_4, XCO_2	0.8	0.4
MERLIN	2021/22	ss	28	global	yes	0.15	active Lidar	1650	XCH_4	n.o.	1 - 2
GEO-CAPE	2022	gs	< 1	continental	yes	0.375	passive UV/VNIR/SWIR	340, 1100, 1245, 1640, 2135	i.a. XSO_2, XHCHO, XCH_4, XNH_3	4.0	n.o.
GeoFTS	proposed	gs	< 1	continental	no	2.7	passive NIR/SWIR	760, 1600, 2300	XCO_2, XCH_4, XCO, XH_2O	0.61	0.2 - 2
geoCARB	2020 - 2023	gs	< 1	continental	no	5 - 10	passive NIR/SWIR	763, 1611, 2065, 2323	XCO_2, XCH_4, XCO	4.0	0.7 - 10
G3E	proposed	gs	< 1	continental	yes	2 x 3	passive NIR/SWIR	760, 1600, 2300	XCO_2, XCH_4, XCO	1.3	0.5 - 10
Sentinel-4/UVN	2019	gs	< 1	national	no	8	passive UV/VNIR	305, 500, 760	XO_3, XNO_2, XSO_2 and XHCHO	n.o.	n.o.
AIRS	2002	ss	0.5	global	no	45	passive TIR	6200, 8200	XO_3, XSO_2, XCO, XCH_4, XCO_2	n.o.	1.5
IASI	2007	ss	0.5	regional/global	no	12	passive TIR	7100, 8300	XO_3, XCH_4, XCO_2, XH_2O	n.o.	1.2
IASI-NG	2021	ss	0.5	regional/global	no	12	passive TIR	7100, 8300	XO_3, XCH_4, XCO_2, XH_2O	n.o.	n.o.
CrIS	2011	ss	0.5	global	no	14	passive TIR	7300, 8000	XCH_4	n.o.	1.5

[95] ss = sun synchronous; gs = geostationary
[96] temporal coverage [days]
[97] ability of point source detection
[98] ground sampling distance [km]
[99] detection threshold [th^{-1}]
[100] retrieval precision [%]
[101] no information

Appendix B: Sectoral Summary Table

Sector (down) Feature (right)	Affected region (large contrast in color)	Characteristic color/shape (specify what it is)	Circular basin	Coal Stockpiles	Conveyor Belts	Disposal site	Machinery (Excavators, Pumps, Power equipment)	Flares	Large Buildings	Long building structures	Large parking lot	Pipes	Power plant on site or close by
Agriculture													
Livestock									AIR/SAT	AIR/SAT			
Pasture									AIR/SAT				
Heavy Industry													
Aluminum Electrolysis & Exclusion		AIR/SAT		SAT		AIR/SAT	SAT			AIR/SAT			SAT
Cement													
> Cement with Quarrying on-site	AIR			SAT			SAT		AIR/SAT				SAT
> Only cement production				SAT			SAT		AIR/SAT				SAT
Chemicals & Industrial Processes				SAT				AIR				SAT	SAT
Oil Refining and Upgrading													SAT
Pulp & Paper													
> Paper and Allied Products				AIR/SAT									
> Printing, Publishing, Allied Industries													
Glass				SAT						AIR/SAT			SAT
Iron & Steel				AIR/SAT				AIR	AIR/SAT				

Color Scheme	
	Not Visible
AIR	Visible through aerial imagery only (access to high resolution satellite data could change this)
SAT	Visible through satellite imagery only (specify)
AIR / SAT	Visible through aerial and satellite imagery (specify satellite)

Usefulness grade	
	very useful
	moderately useful
	not useful

Sector (down) Feature (right)	Pump Jacks	Raw Material Stockpiles (describe)	Rinsing Pools/Basins	Seaside location	Solar PV cells	Specific pattern (Specify)	Storage Tanks	Chimney(s)	Towers	Rail tracks	Trucks	Uban Area	Wastewater treatment and collection basins	Water bodies (lakes, pools)	Wind Turbines
Agriculture															
Livestock													SAT		
Pasture													SAT		
Heavy Industry															
Aluminum Electrolysis & Exclusion				AIR/SAT											
Cement															
> Cement with Quarrying on-site															
> Only cement production															
Chemicals & Industrial Processes							SAT	SAT						SAT	
Oil Refining and Upgrading							AIR/SAT	SAT	SAT						
Pulp & Paper															
> Paper and Allied Products		AIR/SAT											SAT		
> Printing, Publishing, Allied Industries															
Glass								SAT							
Iron & Steel															

Color Scheme	
	Not Visible
AIR	Visible through aerial imagery only (access to high resolution satellite data could change this)
SAT	Visible through satellite imagery only (specify)
AIR / SAT	Visible through aerial and satellite imagery (specify satellite)

Usefulness grade	
	very useful
	moderately useful
	not useful

Sector (down) Feature (right)	Affected region (large contrast in color)	Characteristic color/shape (specify what it is)	Circular basin	Coal Stockpiles	Conveyor Belts	Disposal site	Machinery (Excavators, Pumps, Power equipment)	Flares	Large Buildings	Long building structures	Large parking lot	Pipes	Power plant on site or close by
Mining													
Bauxite	AIR	AIR/SAT					SAT						
Coal	AIR			AIR/SAT	SAT		SAT					SAT	
Gold	AIR					SAT							
Uranium	AIR					SAT							
Iron Ore	AIR					SAT							
Diamond	AIR		SAT										
Oil & Gas Extraction													
Oil production	SAT		AIR/SAT				SAT	AIR					
Power Sector													
Coal				AIR/SAT									
Gas													
Oil												SAT	
Nuclear							SAT						
Renewables	AIR/SAT												
Retail & Commercial													
Wholesale & Retail									SAT		SAT		
Other													

Color Scheme	
	Not Visible
AIR	Visible through aerial imagery only (access to high resolution satellite data could change this)
SAT	Visible through satellite imagery only (specify)
AIR / SAT	Visible through aerial and satellite imagery (specify satellite)

Usefulness grade	
	very useful
	moderately useful
	not useful

Sector (down) Feature (right)	Pump Jacks	Raw Material Stockpiles (describe)	Rinsing Pools/Basins	Seaside location	Solar PV cells	Specific pattern (Specify)	Storage Tanks	Chimney(s)	Towers	Rail tracks	Trucks	Uban Area	Wastewater treatment and collection basins	Water bodies (lakes, pools)	Wind Turbines
Mining															
Bauxite															
Coal			SAT			SAT				SAT	SAT			AIR/SAT	
Gold			AIR/SAT												
Uranium			AIR/SAT												
Iron Ore			AIR/SAT												
Diamond															
Oil & Gas Extraction															
Oil production	SAT			SAT			AIR/SAT								
Power Sector															
Coal								SAT							
Gas							SAT	SAT							
Oil							AIR/SAT								
Nuclear						SAT									
Renewables					AIR/SAT	AIR	SAT	SAT							SAT
Retail & Commercial															
Wholesale & Retail					SAT							SAT			
Other															

Color Scheme	
	Not Visible
AIR	Visible through aerial imagery only (access to high resolution satellite data could change this)
SAT	Visible through satellite imagery only (specify)
AIR / SAT	Visible through aerial and satellite imagery (specify satellite)

Usefulness grade	
	very useful
	moderately useful
	not useful

Oxford Sustainable Finance Programme
Smith School of Enterprise and the Environment
University of Oxford
South Parks Road
Oxford, OX1 3QY
United Kingdom

E enquiries@smithschool.ox.ac.uk
T +44 (0)1865 614942
F +44 (0)1865 614960
www.smithschool.ox.ac.uk

SUSTAINABLE FINANCE PROGRAMME
SSEE

UNIVERSITY OF OXFORD